frontiers | Frontiers in Marine Science

TYPE Original Research
PUBLISHED 11 November 2024
DOI 10.3389/fmars.2024.1464653

OPEN ACCESS

EDITED BY
Michele Giani,
National Institute of Oceanography and Applied Geophysics, Italy

REVIEWED BY
Matthew Buckley Alkire,
University of Washington, United States
Thiago Monteiro,
Universidade Federal do Rio Grande, Brazil

*CORRESPONDENCE
Karol Kuliński
kroll@iopan.pl

RECEIVED 14 July 2024
ACCEPTED 17 October 2024
PUBLISHED 11 November 2024

CITATION
Aguado Gonzalo F, Stokowski M, Koziorowska-Makuch K, Makuch P, Beszczyńska-Möller A, Kukliński P and Kuliński K (2024) Key processes controlling the variability of the summer marine CO_2 system in Fram Strait surface waters. *Front. Mar. Sci.* 11:1464653. doi: 10.3389/fmars.2024.1464653

Key processes controlling the variability of the summer marine CO_2 system in Fram Strait surface waters

Fernando Aguado Gonzalo[1], Marcin Stokowski[2], Katarzyna Koziorowska-Makuch[1], Przemysław Makuch[3], Agnieszka Beszczyńska-Möller[3], Piotr Kukliński[4] and Karol Kuliński[1]*

[1]Department of Marine Chemistry and Biochemistry, Institute of Oceanology of the Polish Academy of Sciences, Sopot, Poland, [2]Department of Genetics and Marine Biotechnology, Institute of Oceanology of the Polish Academy of Sciences, Sopot, Poland, [3]Department of Physical Oceanography, Institute of Oceanology of the Polish Academy of Sciences, Sopot, Poland, [4]Department of Marine Ecology, Institute of Oceanology of the Polish Academy of Sciences, Sopot, Poland

The aim of this study was to decouple and quantify the influence of various biological and physical processes on the structure and variability of the marine carbonate system in the surface waters of the eastern part of the Fram Strait area. This productive region is characterized by its complex hydrographic and sea ice dynamics, providing an ideal set up to study their influence on the variability of the marine carbonate system. Different variables of the marine CO_2 system: Total Alkalinity (TA), Dissolved Inorganic Carbon (DIC), partial pressure of CO_2 (pCO_2), and pH, were analysed together with temperature, salinity, sea ice extension, and chlorophyll *a* distribution during three consecutive summers (2019, 2020 and 2021), each of them having a unique oceanographic setting. The data revealed that TA and DIC are mostly controlled by the mixing of Atlantic water and sea ice meltwater. The combined effects of organic matter production/remineralization, calcium carbonate precipitation/dissolution, and air/sea CO_2 gas exchange cause deviations from this salinity-related mixing. The scale of these deviations and the proportion between the effects observed for TA and DIC suggest interannual shifts in net primary production and dominant phytoplankton species in the area. These shifts are correlated with the sea ice extent and the spread of the Polar Surface Waters in the region. Net primary production is the main factor controlling the temporal and spatial variability of pH and pCO_2 in the study area followed by the influence of temperature and, mixing of water masses expressed with salinity (seawater freshening). Surface waters of the Fram Strait area were generally undersaturated in CO_2. The lowest pCO_2 values, coinciding with an increase in oxygen saturation, were observed in areas of mixing of Arctic and Atlantic-derived water masses. However, as shown for 2021, a reduction of the sea ice extent may induce a westward shift of the chlorophyll maximum, resulting in pCO_2 increase and pH decrease in the eastern part. This indicates that sea ice extent and associated spread of Polar Surface Waters may be important factors shaping primary production, and thus pCO_2 and pH, in the Fram Strait area.

KEYWORDS

Marine CO_2 system, Arctic, Fram Strait, ocean acidification, pCO_2, pH, sea ice

1 Introduction

Due to climate change driven by anthropogenic forces, the Arctic Ocean is experiencing fast warming (Meredith et al., 2019). The sea ice concentration and extension in the Arctic have recently radically decreased in response to the increase in temperatures (Carmack et al., 2016; Comiso et al., 2011; Haine et al., 2015; Stroeve et al., 2012), and according to some future climate projections it may seasonally even completely disappear by mid-century (Peng et al., 2020). One of the expected consequences is the expansion of open waters favouring the air-sea CO_2 interchange. Up to today, between 116 ± 4 and 166 ± 60 TgC yr^{-1} of atmospheric CO_2 is being taken up by the Arctic Ocean (MacGilchrist et al., 2014; Yasunaka et al., 2023). Consequently, the uptake of CO_2 by the ocean is changing seawater chemistry, increasing dissolved inorganic carbon (DIC) concentration and reducing pH and calcium carbonate saturation state (Ω) (Ahmed et al., 2020; Bates and Mathis, 2009; Caldeira and Wickett, 2003; Manizza et al., 2019; Yasunaka et al., 2016), a process commonly known as Ocean Acidification (OA), which represents a direct threat to calcifying organisms (Wittmann and Pörtner, 2013; Kleypas, 2019).

The high solubility of CO_2 in cold polar regions makes them especially sensitive to ocean acidification, particularly in areas influenced by deep water upwelling (Qi et al., 2022), river runoff (Capelle et al., 2020; Fransson et al., 2009; Koziorowska-Makuch et al., 2023; Woosley and Millero, 2020), and sea-ice melting (Tynan et al., 2016; Zhang et al., 2020), with the latter two processes also reducing the buffer capacity of surface waters, inducing rapid pH changes. Moreover, the influence of sea-ice meltwater in surface waters enhances stratification, reducing vertical fluxes of nutrients and carbon, which has a direct impact on primary producers and CO_2 uptake and sequestration (e.g. Tremblay et al., 2015). Quick ice-melting events during summer are expected to become more frequent in the following decades due to the overall Arctic warming and the thinning of sea ice (e.g., Stroeve and Notz, 2018, and references therein), enhancing the influence of freshened, low alkalinity Arctic surface waters.

Moreover, the annual net primary production (NPP) in the Arctic Ocean has increased in the last decades (Lewis et al., 2020), a phenomenon that has been associated mostly with the expansion of open waters due to the sea ice loss (Carmack et al., 2016; Comiso et al., 2011; Haine et al., 2015; Stroeve et al., 2012). Corresponding to this change, biologically driven processes, such as primary production (PP) and remineralization of organic matter (OM), as well as the formation and dissolution of calcium carbonate, have a strong influence on all parameters of the carbonate system (Chierici et al., 2019; Wolf-Gladrow et al., 2007 and references therein), being especially important for CO_2 partial pressure (pCO_2) of surface waters and thus anthropogenic carbon sequestration (Devries, 2022 and references therein).

This all shows a strong interconnection between Arctic warming, sea ice extent, and NPP, and all these processes directly influence the marine carbonate system. Therefore, to estimate and project future changes in carbon sequestration and ocean acidification, it is necessary to understand and quantify spatial and temporal variations in the marine CO_2 system caused by these main drivers.

One of the most biologically productive sectors in the Arctic region is the Fram Strait area (Pabi et al., 2008; Slagstad et al., 2015). Being also the main gateway for sea ice export from the Arctic (e.g., Spreen et al., 2020), it provides a unique setting to study the influence of the changes in the cryosphere and the biological processes on the variability of the marine carbonate system in the surface waters. Furthermore, it was already reported that factors controlling changes in Fram Strait NPP are potentially associated with variations in ice-free zones during the growing season (Kahru et al., 2011; Arrigo and van Dijken, 2015), intensification of the water column stratification due to increased ice melting (Mayot et al., 2020), rising sea surface temperature (SST) (Cherkasheva et al., 2014), increase in nutrients availability (Krisch et al., 2020; Tuerena et al., 2021), and changes in the dynamics of the water masses (Arrigo et al., 2017; Joli et al., 2018; Marchese et al., 2019).

However, Fram Strait is also the main gateway for water masses and heat exchange between the Arctic Ocean and the North Atlantic (Beszczynska-Möller et al., 2012). The distribution of water masses and their interactions in Fram Strait are mainly controlled by the East Greenland Current (EGC) and the West Spitsbergen Current (WSC) (e.g., Beszczynska-Möller et al., 2012). The EGC brings cold and low saline waters and sea ice southward from the Arctic and follows the shelf slope east of Greenland (Halvorsen et al., 2015; Håvik et al., 2017). The WSC carries warm and more saline Atlantic-origin waters (AW) northward above the shelf break and continental slope along the western Spitsbergen coast. Although these main flows set up the water mass circulation in the area (Beszczynska-Möller et al., 2012), salinity distribution in the first meters of the water column is further modified by regional winds (Tsukernik et al., 2010; Halvorsen et al., 2015), storms (Brümmer et al., 2001; Graham et al., 2019), mesoscale eddies (Hattermann et al., 2016), sea ice melt (Marnela et al., 2013), recirculation of Atlantic Water (de Steur et al., 2014; Hattermann et al., 2016; Marnela et al., 2013; Richter et al., 2018; Hofmann et al., 2021) and evaporation-precipitation balance (Vihma et al., 2016). This complex oceanographical setup produces an intense spatial and temporal variation in NPP (Cherkasheva et al., 2014; Mayot et al., 2020), sea ice dynamics (Halvorsen et al., 2015; Spreen et al., 2020) and planktonic communities (Nöthig et al., 2015 and references therein), which add on top to the complexity of the carbonate system in the region and make understanding its spatio-temporal variability a challenging task.

The main goal of this study was to decouple and quantify the influence of various biological and physical processes on the structure of the marine carbonate system in the eastern Fram Strait surface waters, including its spatial and interannual variability. This was done by interpreting the results of the marine carbonate system from summer seasons of three consecutive years, each of which was analysed against the background of a unique oceanographical setting such as distribution of surface salinity and temperature, sea ice extent, as well as chlorophyll *a* distribution. The first part of the manuscript presents changes in total alkalinity (TA) and DIC, with particular emphasis on how biological processes may influence them. The

second part focuses on understanding and quantifying the main pH and pCO_2 distribution drivers and their spatial variability. The last part presents two hypothetical future scenarios, the first one where the surface waters are highly influenced by meltwater from sea ice and the second one with reduced influence of melted sea ice, providing an understanding of how the warmer, fresher, and sea-ice-reduced future will influence the marine carbonate system in the Fram Strait surface waters.

2 Methods

2.1 Sampling

In 2019, 2020, and 2021, biogeochemical and hydrographic data were collected from surface waters during the annually repeated research cruises of RV Oceania under the Institute of Oceanography Polish Academy of sciences (IOPAN) long-term Arctic research monitoring program (AREX). The sampling area covered the eastern part of the Fram Strait (Figure 1) extending from the west coast of Svalbard to approximately the Greenwich meridian and crossing the West Spitsbergen Current. The cruises of 2019 and 2021 were carried out from 21st June to 21st July, and in 2020, sampling was realized two weeks later, due to restrictions related to the Covid-19 pandemic, from 6th July to 8th August, all coinciding with the high melting season.

Surface seawater from a depth of 2.5 m was supplied with a specially designed, and previously used by Stokowski et al. (2021), plumbing system to the vessel's laboratories for both underway continuous measurements (salinity, temperature, pCO_2, oxygen saturation – O_2, and pH) and for collecting discrete samples for TA and DIC. The underway measurements of salinity, temperature, pCO_2 and O_2 were taken at a one-minute resolution along the cruise route, except for the year 2020, when salinity and temperature data (due to the malfunctioning of the thermosalinograph) were extracted from approx. 270 CTD profiles, taken at regular grid within the sampling trajectory of the RV Oceania (Figure 1). The set of high-resolution measurements was completed with pH measured every 30 minutes. To allow comparing the spatial pH, pCO_2, O_2, T and Sal distribution from different years and to calculate the average values for each of them, all measurements collected for each year were interpolated over a regular grid with a resolution of 0.002° x 0.007° (latitude x longitude) using the weighted-average gridding from Ocean Data View (Schlitzer, 2023).

In addition to the underway measurements, samples for TA and DIC were collected using 250 mL borosilicate bottles at approximately 30 stations homogeneously distributed across the sampling area (Figure 2). Immediately after sampling they were preserved using 100 µL $HgCl_2$ and stored in a refrigerator (between 2 and 5 °C) until they were analysed in the IOPAN laboratories.

Moreover, seawater sampling was supplemented by estimating the sea ice extent for the date when half of the sampling cruise was completed. This was done based on the data from the Advanced Microwave Scanning Radiometer 2 (AMSR-2), University of Bremen (seaice.uni-bremen.de, Spreen et al., 2008). The area with more than 10% Sea Ice Coverage (10% SIC) was compared to the total area of the investigated region. This was achieved by measuring the total surface (number of pixels) representing water in the chart and the surface of the area with SIC > 10%, the area was measured in pixels (px^2). The investigated region was defined as the area comprising approximately from the Fram Strait at 81.5°N to 74°N and from the Greenland coast to approximately the east coast of the Svalbard archipelago (-20°W to 25°E). For visual comparison of the SIC conditions in the sampling area, the 10% SIC line was overlaid on spatial maps to indicate the variability of sea ice cover in different years.

The surface chlorophyll distribution maps from July 2019, 2020, and 2021 are a satellite-derived MODIS-Aqua monthly average composite Chlorophyll *a* concentration (mg/m3) (NASA Ocean Biology Processing Group, 2023) retrieved from https://oceancolor.gsfc.nasa.gov/l3/.

2.2 Measurement techniques and laboratory analyses

2.2.1 Salinity and temperature

During 2019 and 2021, salinity and temperature were continuously measured in the flow of surface water using an SBE 21 SeaCAT thermosalinograph (SeaBird) installed on board and equipped with an additional temperature sensor SBE38 located at the water inlet, both sensors were calibrated in every cruise shortly before starting it. The temperature accuracy was ± 0.01°C in both instruments and the initial accuracy conductivity of the SBE 21

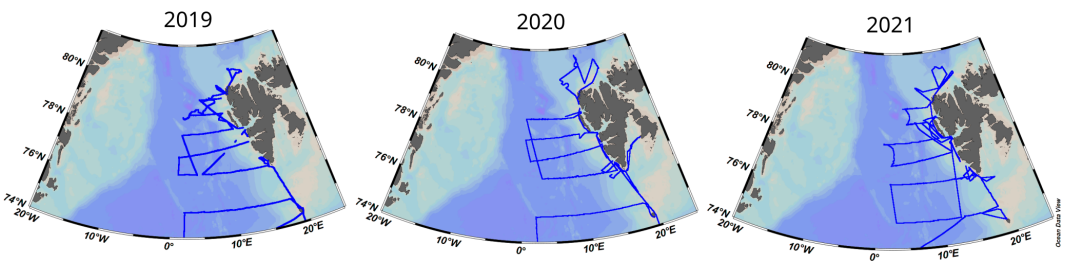

FIGURE 1
Location of the sampling area. The blue lines represent the trajectory of the RV Oceania, where continuous measurements were taken (temperature, salinity, pH, pCO_2, and O_2). Figure created with Ocean Data View (Schlitzer, 2023).

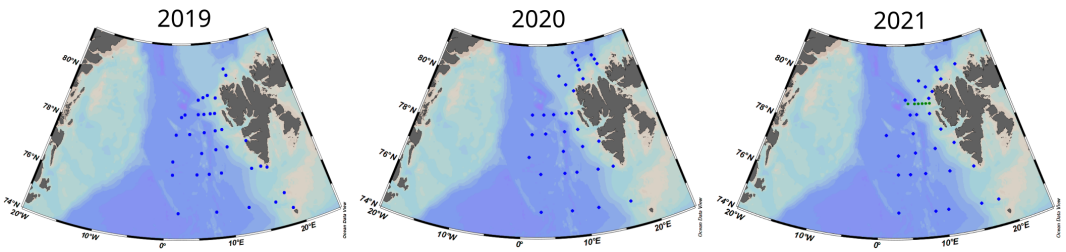

FIGURE 2
Study area with the location of the TA and DIC sampling locations (blue dots) during 2019, 2020 and 2021. The green dots in 2021 (right) show the location of the water column profiles extracted from the "CarbonBridge productivity regimes in the Arctic Ocean" project dataset (Paulsen et al., 2017) collected in January 2014. Figure created with Ocean Data View (Schlitzer, 2023).

SeaCAT-thermosalinograph was ± 0.001 S/m. In 2020, the surface salinity and temperature data were derived from CTD casts taken with the SBE9/11+ system (SeaBird) installed on a water carousel, which was calibrated shortly before the beginning of the cruise with a temperature (conductivity) accuracy of 0.01°C (± 0.001 S/m). All data was averaged using the same grid resolution as explained in section 2.1.

2.2.2 Partial pressure of CO_2

The pCO_2 was measured with a precision/accuracy of 1.3 µatm using a system equipped with a cavity ring-down spectroscope (CRDS) G2101-i (Picarro) connected to a bubble-type equilibrator with an additional spray-type water diffuser (see Stokowski et al., 2021 for a detail description of the method). The quality of the CRDS was assured by regular measurements of pure nitrogen (Linde 5.0) and artificial air with 205 and 507 ppm of CO_2. The temperature difference between the water inlet and equilibrator was corrected using the relationship between temperature and pCO_2 proposed by Takahashi et al. (1993).

2.2.3 Oxygen saturation

The O_2 measurements were performed in the same equilibrator as for pCO_2 using a Fibox 4 equipped with a dipping optode (PreSens GmbH, Germany). The optical sensor was calibrated using N_2 and ambient air. The response time was set to 10 seconds, and the measurements assured the precision of ± 0.3% of the saturation values.

2.2.4 pH

The pH was measured using the HydroFIA pH spectrophotometric system (CONTROS, 4H-JENA Engineering GmbH) from the same surface water flow used for other underway measurements. The quality of pH results was proved with repeated measurements (at 25°C) of the certified TRIS buffer (TRIS-CRM-T37) provided by A.G. Dickson (Scripps Institution of Oceanography, USA). The instrument yielded a precision of 0.002 pH units and an accuracy of 0.003.

2.2.5 Dissolved inorganic carbon

DIC samples from 2019 were measured on a Shimadzu TOC-L analyzer at the Institute of Oceanology of the Polish Academy of Sciences (IO PAN) in Poland. Samples collected in 2020 were measured at the Helmholtz-Zentrum Hereon (Germany) using a VINDTA 3C (Versatile INstrument for the Determination of Total dissolved inorganic carbon and Alkalinity) based on coulometric titration (Johnson et al., 2000). The samples collected in 2021 were measured on an automated DIC AS-C6L analyzer (Apollo SciTech) at the IOPAN.

2.2.6 Total alkalinity

The analysis of the samples collected in 2019 and 2021 for TA was made on an automated, open-cell potentiometric titration system developed by Andrew Dickson (Scripps Institution of Oceanography/UCSD, USA) (Dickson et al., 2007), while in 2020 using VINDTA 3C based on close-cell potentiometric titration.

For all DIC and TA measurements, the accuracy was ensured using certified reference materials (CRMs, batches no. #190 and #195) from A.G. Dickson (Scripps Institution of Oceanography, USA). These were also used for quantification of the precision for each of the used instruments, which was not worse than ± 3 µmol kg^{-1} for DIC and ± 4 µmol kg^{-1} for TA.

2.3 Calculations of the marine carbonate system.

Quantifying the influence of different biological and physical parameters on the marine CO_2 system was done for sampling locations for which the complete data set was collected, including DIC, TA, pH, pCO_2, salinity, and temperature. The computations of the carbonate system were done using version 2.3 of the CO2SYS program for Excel (Microsoft) (Lewis et al., 1998). Previous studies (Chen et al., 2015; Chierici and Fransson, 2009; Raimondi et al., 2019; Woosley et al., 2017) suggested that the carbonic acid dissociation constants guaranteeing the best consistency between calculations and observations of the marine CO_2 system in the Arctic waters are these by Mehrbach et al. (1973) as refitted by Dickson and Millero (1987) (later referenced as MER) and Lueker et al. (2000). Following these recommendations, and in agreement with Tynan et al. (2016), the carbonic acid dissociation constant of MER was selected.

The complete set of dissociation constants used in the computations included: MER for carbonic acid, Dickson et al. (1990) for HSO_4^-, Perez and Fraga (1987) for HF, and Dickson

et al. (1990) for borates. Additionally, boron concentrations have been approximated in the CO2SYS with the dependency by Lee et al. (2010), and the pH was reported on the total scale (pH = $-\log_{10}$ ($[H^+]$ + $[HSO_4^-]$) corresponding to our measurement technique.

2.3.1 Interannual biogeochemical variability

In order to compare biogeochemical changes between different years, it is necessary to select a reference value from which the annual change could be estimated. Therefore, the averages of the physical and chemical properties from the first 50 m of the Surface Winter Waters (SWW) in Fram Strait (Figure 2) were compared to the data obtained in this study during consecutive summers. The comparison of biogeochemical properties between winter (or pre-bloom) and summer (or post-bloom) waters has been used as a tool for tracing and quantifying biogeochemical changes in the area (e.g., Chierici et al., 2019). As the goal of this study was to compare the relative changes in the biogeochemistry of the entire region between consecutive years rather than to provide a net quantification of different biogeochemical processes at each sampling location, the SWW can be considered as a semi-arbitrary reference point to estimate the relative differences with respect to this point, giving simultaneously a tool to compare data collected during different years. A unique aspect of this approach is the possibility of quantifying the biogeochemical variability within the study area using the same reference point (for example, how latitudinal changes in temperature may influence pH in different years having different temperature gradients), but also considering the uncertainties that entail.

The winter data of temperature, salinity, TA, and DIC ($Temp_{wv}$, Sal_{wv}, DIC_{wv}, TA_{wv}) collected in January 2014 were obtained from the "CarbonBridge productivity regimes in the Arctic Ocean" project dataset (Paulsen et al., 2017). As presented before, these data do not represent the characteristics of the entire area but rather a semi-arbitrary point to compare biogeochemical differences between years. The mean values in the upper 50 m were obtained by averaging all the data from 2, 5, 11, 20, 30, and 50 m water depths from six water column profiles taken perpendicular to the west coast of Svalbard (see Figure 2 for more details). Furthermore, using the same dataset (Paulsen et al., 2017), the average values for the surface water layer (upper 50 m) have been compared with averages for 500 m (Table 1) and also with data collected below the photic zone (between 100 and 400 m) at selected locations during the 2021 sampling campaign (see Supplementary Table S1 for more details). The standard deviation for TA and DIC, between the three datasets mentioned in Table 1, was ± 4 µmol kg^{-1} for both of them (DIC and TA), which suggests a relative homogeneity of DIC and TA in the upper 500 m of water column after winter mixing and relatively small (negligible) interannual variability of DIC and TA in the region. Still, however, our data was only collected during one year (2021) and does not necessarily represent the values of TA and DIC from 2019 and 2020 which we cannot confirm to be within the variability of the already presented data.

The values of pCO_2 and pH (pCO_{2wv}, pH_{wv}) for SWW were calculated using version 2.3 of the CO2SYS program for Excel (Microsoft) (Lewis et al., 1998) using as input values $Temp_{wv}$, Sal_{wv}, DIC_{wv}, TA_{wv}.

2.3.2 Sea-ice as marine CO_2 system end member

During spring and summer, the winter water mixes in the surface layer mainly with sea ice meltwater (see section 3.1 for more details). To estimate TA and DIC changes due to this effect, the end member values of DIC_{ice} (355 ± 75 µmol kg^{-1}), TA_{ice} (441 ± 52 µmol kg^{-1}), and salinity (Sal_{ice} = 5.0 ± 0.9) for sea-ice were obtained from the study by (Rysgaard et al., 2007). These values have been obtained by averaging the results from 5-10 cm thick layers extracted from nine sea ice cores (0.9-1.9 m long), collected in Franklin Bay, N Canada (70°N, 126°W) in April 2004 and Young Sound, NE Greenland (74°N, 20°W) in March 2005. A detailed description of the methodology used during sampling and all the sea ice data is reported in Rysgaard et al. (2007).

2.3.3 Seasonal variations of TA and DIC

Relative changes in DIC and TA due to the mixing effect of SWW with sea ice meltwater (defined as DIC_{sal} and TA_{sal}) can be calculated as a function of salinity and expressed as a linear correlation between the two end members: sea surface DIC and TA during winter (DIC_{wv}, TA_{wv}) and melted sea ice (DIC_{ice}, TA_{ice}). TA_{sal} and DIC_{sal} at each sampling station can be calculated using Equations 1, 2.

$$TA_{sal} = 62.468 * (salinity) + 125.92 \quad (1)$$

TABLE 1 Average values of different parameters measured in the Fram Strait area during the winter of 2014 (Paulsen et al., 2017) Surface winter 2014 (SWW) is the average value of the first 50 m of the water column, while 500m winter 2014 is the value measured at 500 m at different locations of the sampling area (Figure 1). 100-400m summer 2021 are the average values from 16 measurements taken during the sampling campaign in 2021 at different depths (between 100 and 400 m), for more information see Supplementary Material (Supplementary Table S1).

	Salinity	Temperature (°C)	TA (µmol kg^{-1})	DIC (µmol kg^{-1})	pH (total scale)	pCO_2 (µatm)	Notation
Surface winter 2014	34.96	3.15	2309	2159	8.065	366	WW
500m winter 2014	35.06	2.90	2311	2166			$W14_{500}$
100-400m summer 2021	34.97	2.37	2301	2168			

$$DIC_{sal} = 60.367 * (salinity) + 49.052 \quad (2)$$

Therefore, the difference between TA and DIC measured in the consecutive summers (TA_{meas}, DIC_{meas}) and the calculated effect of mixing with meltwater (TA_{sal} and DIC_{sal}) should be the accumulated result of biological processes and air-sea CO_2 interchange (ΔTA_{bio} and ΔDIC_{bio}).

$$\Delta TA_{bio} = TA_{meas} - TA_{sal} \quad (3)$$

$$\Delta DIC_{bio} = DIC_{meas} - DIC_{sal} \quad (4)$$

2.3.4 Calculations of pH variations

Winter-to-summer changes in pH and pCO_2 were attributed to several processes: temperature (temp), inputs of freshwater from ice melting (sal), biological processes plus air-sea CO_2 fluxes (bio), and inconsistencies (inc). Variations in pH were calculated in CO2SYS using different combinations of the SWW variables reported in Table 1 ($Temp_{wv}$, Sal_{wv}, DIC_{wv}, TA_{wv}) and values obtained in this study for consecutive summers (TA_{meas}, DIC_{meas}, pCO_{2meas}, pH_{meas}, $temp_{meas}$, and sal_{meas}).

Changes in pH due to temperature variations (ΔpH_{temp}) were calculated assuming that temperature is the only variable changing between winter and summer. Thus, ΔpH_{temp} (Equation 5) was determined as the difference between winter pH (pH_{wv}, Equation 6) and the pH calculated as a function of winter salinity, DIC, and TA (Sal_{wv}, DIC_{wv}, TA_{wv}) and the measured temperature during summer.

$$\Delta pH_{temp} = pH_{calc} \quad f(temp_{meas}, sal_{wv}, DIC_{wv}, TA_{wv}) - pH_{wv}; \quad (5)$$

$$\text{Where } pH_{wv} = pH_{calc} \quad f(temp_{wv}, sal_{wv}, DIC_{wv}, TA_{wv}) \quad (6)$$

The influence of sea ice meltwater can change salinity and, therefore, TA and DIC in the surface waters, influencing pH. Thus, the pH changes due to the physical mixing of water masses (ΔpH_{sal}) were determined by subtracting the winter pH (pH_{wv}) from the theoretical pH_{sal} calculated by applying winter temperature ($Temp_{wv}$), summer salinities (sal_{meas}) and related to these salinities TA_{sal} and DIC_{sal} obtained from Equations 1, 2, respectively:

$$\Delta pH_{sal} = pH_{sal} - pH_{wv}; \quad (7)$$

$$\text{Where } pH_{sal} = pH_{calc} \quad f(temp_{wv}, sal_{meas}, DIC_{sal}, TA_{sal}) \quad (8)$$

The difference between TA and DIC measured in the consecutive summers (TA_{meas}, DIC_{meas}) and TA_{sal} and DIC_{sal} (Equations 1, 2) resulting from the physical mixing of water masses (or the influence of sea ice melting) can be attributed to the total effect of both biological processes (photosynthesis/respiration and calcification) and sea-air CO_2 exchange. Thus, the accumulated pH change corresponding to these effects (ΔpH_{bio}) can be calculated as:

$$\Delta pH_{bio} = pH_{calc} \quad f(temp_{wv}, sal_{meas}, DIC_{meas}, TA_{meas}) - pH_{sal} \quad (9)$$

To evaluate the consistency of the marine CO_2 system data presented in this study, the calculated pH from $temp_{meas}$, sal_{meas}, DIC_{meas}, and pCO_{2meas} was compared to the measured pH (pH_{meas}). The differences were attributed to the error propagation during calculations (Orr et al., 2018) and chemical components that may affect the equilibrium of the marine CO_2 system but are not yet parametrized in the mass balance equations used in the calculations (e.g., Kuliński et al., 2017)

$$pH_{inc} = pH_{calc} \quad f(temp_{meas}, Sal_{meas}, DIC_{meas}, pCO_{2meas}) - pH_{meas} \quad (10)$$

3 Results and discussion

3.1 Oceanographical settings

Surface temperature and salinity in the entire studied area during three years (2019, 2020, 2021) ranged between -0.5 and 8.5°C and between 30.0 and 35.2, respectively (Figures 3A, B). However, lower salinities were occasionally observed close to the ice margin. Sea surface salinity in the investigated area had generally quite similar distribution every year (Figure 3A). Warmer and more saline waters were found in this region in the southern part, which is related to the transformation of Atlantic Water during its northward transport in the WSC (Figure 4) (Hattermann et al., 2016). This effect was well reflected in our data by a surface patch of more saline waters extending northward and centred at 10°E. As AW flows northwards, surface waters experience intense cooling and freshening; the heat released during cooling enhances sea ice melting (Polyakov et al., 2010; Rippeth et al., 2015). Two frontal zones with stronger salinity and temperature gradients were identified in the surface layer based on the analyzed data set. One of them extending along the west coast of Svalbard represents the West Spitsbergen Polar Front (Nilsen et al., 2016) which separates Atlantic water in the WSC ($S > 34.8$) from the colder and fresher Arctic-type water ($S < 34.8$) originating from the South Cape Current (SCC) and carried northward along the West Spitsbergen shelf (Figure 4) (Saloranta and Svendsen, 2001; Nilsen et al., 2021). The second salinity/temperature front, which reflects a boundary between Atlantic and Polar waters in Fram Strait (Karpouzoglou et al., 2022), more winding, was located along the sea-ice margin with slight shifts from year to year, depending on the sea ice extension (Figure 3A). To determine the location of this front during different years we selected the isohaline 34.8 which coincides with the boundary of the frontal area with a strong salinity gradient in our data. In the central Fram Strait, it depicts the transition zone between the northward flowing Atlantic Water and Polar Water (PW) originating in the Arctic Ocean and carried southward by the East Greenland Current. Therefore, it can be considered an excellent tool to compare the front extension during consecutive years. As illustrated in Figure 3A, a smaller extension of the isohaline 34.8 was observed in 2021 compared to 2020 and 2019, which coincides well with the sea ice extension in the region. During

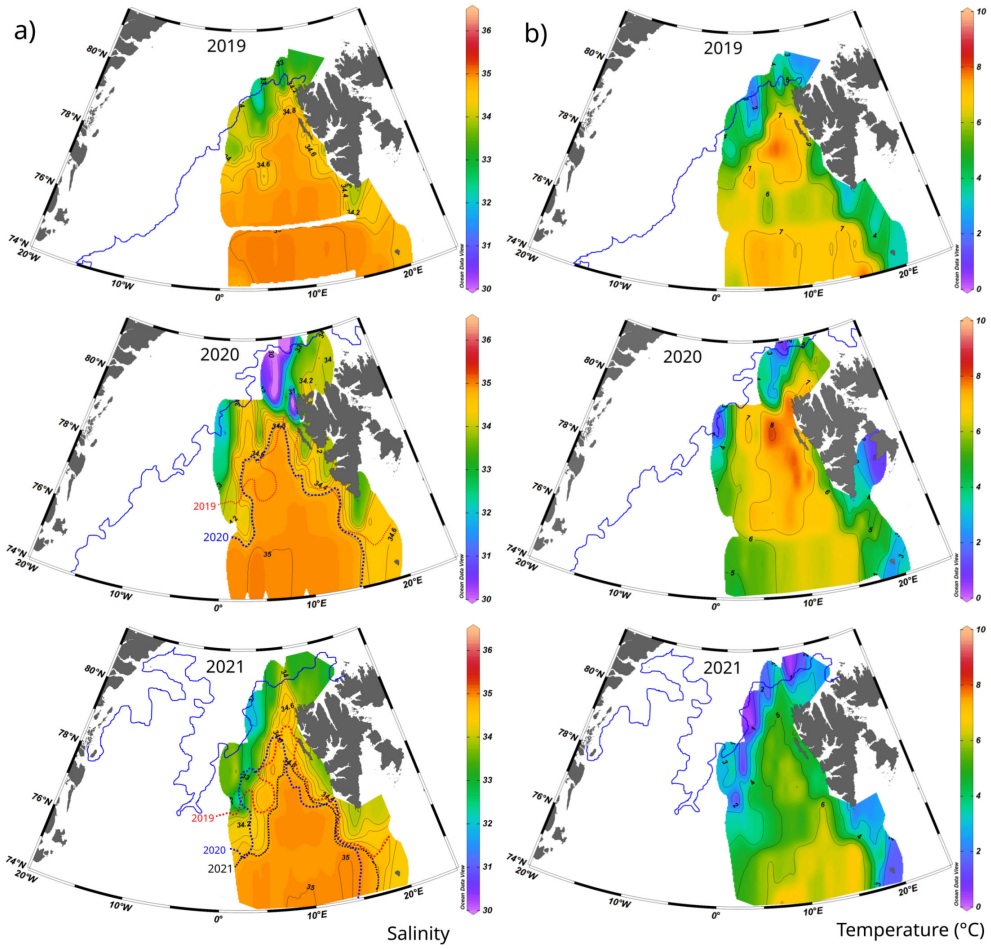

FIGURE 3
Surface salinity **(A)** and temperature **(B)** distribution in the study area during 2019, 2020 and 2021. As a reference, the isoline of 34.8 from previous years was marked in the salinity maps. The original surface data was extrapolated using the weighted-average gridding from Ocean Data View (Schlitzer, 2023). The blue line represents the 10% sea ice coverage (SIC), northern of this line the SIC is higher than 10%. The study area covered by SIC higher than 10% was 49.94% during 2019, 32.69% in 2020 and 18.68% in 2021. Detailed maps presenting the SIC are shown in the Supplementary Material (Supplementary Figure S1).

these three years, there was a strong variability in the area covered with sea ice as expressed with SIC higher than 10% (SIC > 10%). In July 2019 it was 49.94% of the investigated region, while in 2020 and 2021 it was 32.69% and 18.68%, respectively (Figure 3; Supplementary Material S1). The decrease in surface salinity can be linked to enhanced sea ice melting, providing more fresh water to the surface layer, and/or to changes in surface circulation. Unfortunately, our data only provide information on sea ice coverage and the relationship between sea ice melting and corresponding released freshwater volume and surface salinity distribution has to be corroborated in future studies. Independently of the prevailing mechanism, it is clear that the extent of waters with surface salinity higher than 34.8 was reduced in 2021, having thus less impact on surface processes.

Unlike the salinity distribution, the surface temperatures show a strong interannual variability (Figure 3B). A strong temperature gradient was observed in all studied years close to the sea-ice margin in the west/northwest part of the study area, with warmer waters following the direction of the WSC from the south and reaching up to 79°N. Still, the spatially averaged surface temperature (calculated as the average of the gridded data, with the same spatial distribution and the same extension between years, see methods) differed from one year to another, amounting to 5.2°C during 2019, 5.3°C in 2020, and 3.8°C in 2021. The spatial patterns of the temperature gradients also varied between different years. One of the main features that could be distinguished is a zonally extending pattern of lower surface temperature located at 76°N in 2019, at 75°N in 2020, and at 76°N in 2021 (Figure 3B). An explanation of causal mechanisms, responsible for complex and annually varying patterns of surface temperature is beyond this study. However, the average surface temperature clearly shows colder surface waters during 2021 than during 2019 and 2020, coinciding with a smaller extension of the AW surface pattern (defined as surface waters with S > 34.8) and reduced sea ice.

The surface temperature and salinity variability reflect the general large-scale patterns previously described for this area, where warmer and more saline AW is transported northwards in the WSC. As AW flows northward, it mixes with colder and fresher

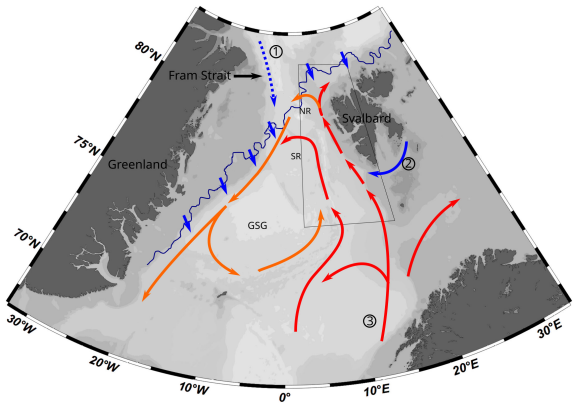

FIGURE 4
Schematic representation of the main surface currents encountered in the study area (based on Hattermann et al., 2016). The blue line represents the limit of the 10% sea-ice concentration (see methods). The black box delimit the study area. The color in the arrows represents a schematic view of the main water masses in the area and its transformations. Blue arrows represent the influence of Arctic waters, either as melted sea ice (small ones), as Arctic surface waters (1) or Arctic waters carried by the South Cape Current (SCC) (2). The red arrows represent the Atlantic Water (AW) carried by the West Spitsbergen Current (WSC) (3), orange Polar warm Surface Waters (PSWw). GSG, NR, and SR denote Greenland Sea Gyre, Northern Recirculation, and Southern Recirculation, respectively.

melted sea-ice waters, creating warm Polar Surface Waters (PSWw) (Rudels et al., 2005). Rudels et al. (2005) define PSWw in terms of temperature and potential density (warmer than 0°C and less dense than 27.7) but for the purpose of this study, we take advantage of the isohaline of 34.8 as a good delimiter of the surface boundary between the Atlantic and Arctic derived waters. Therefore, water with S > 34.8 will be denoted as AW and water with S < 34.8 will be described as PSWw.

PSWw sitting on the top of Atlantic water can flow eastward, following the north Svalbard circulation (Athanase et al., 2020), or westward and then southward along the sea-ice margin zone (Marnela et al., 2013; Hattermann et al., 2016). This recirculation pattern explains the high salinity gradient in our data between the AW flowing northward and PSWw moving southward. However, it was also possible to identify some isolated patches with S > 34.8 outside of the main AW inflow, probably originating from the mesoscale eddies generated in the eastern Fram Strait (Bashmachnikov, 2020; Bashmachnikov et al., 2023; Raj et al., 2016), which bring colder and more saline subsurface Atlantic waters to the surface, breaking the seasonal stratification.

The part of the western branch of the WSC recirculates in Fram Strait mainly along two routes: a Northern Recirculation (NR) around the Molloy Hole near 80°N (Hattermann et al., 2016) (Figure 4) or a Southern Recirculation (SR) located south of 79° N. The SR is mainly related to the eastern rim of the Greenland Sea Gyre (GSG) (de Steur et al., 2014; Beszczynska-Möller et al., 2012) (Figure 4). Variability in the AW temperature reaching the Fram Strait has been associated with changes in the GSG circulation (Chatterjee et al., 2018), where a stronger GSG circulation strengthens the AW inflow along the WSC. It can be reflected in surface waters in the southern Fram Strait, where a stronger GSG promotes a northern extension of the AW which in the upstream area extends to the surface before being transformed in PSWw as it mixes with meltwater.

Hence, interannual and spatial variations in surface temperature and salinities can be explained through changes in surface circulation and varying sea-ice extension and melting rates. Warmer and more saline waters, as observed for 2019 and 2020 (Figures 3A, B), correspond to a higher influence of AW in the surface waters or a reduction of the PSWw. On the other hand, cooler and fresher surface waters, as observed during 2021 along with a decrease in sea-ice extension (which was reduced from 43.94% of the region covered in 2019 to 18.68% in 2021), could be related to a higher volume of sea ice meltwater or/and varying intensity of recirculation, which would explain differences in the sea ice extension and the expansion of the area covered by PSWw.

3.2 The marine carbonate system

3.2.1 Distribution of TA and DIC

The data collected for TA and DIC from 2019 to 2021 are shown in Figure 5. The main changes in TA are closely correlated as a function of salinity. TA data shows a conservative mixing along the line drawn between the AW properties reported for winter (salinity 34.96 and TA = 2310 μmol kg^{-1}, Table 1) and the TA of the melted sea ice (salinity 5.0 and 441 μmol kg^{-1} TA) (see methods for details and references) revealing high variability, but similar to previously reported in the area (Chierici et al., 2019; Tynan et al., 2016). Tynan et al. (2016) were able to characterize two TA_0 zero salinity end-members, one lower (TA_0 = 403 μmol kg^{-1}) associated with sea ice melting and one higher (TA_0 = 1230 μmol kg^{-1}) related to the influence of Polar Waters. However, our data only shows the influence of one TA_0 with low values (~ 420 μmol kg^{-1}), supporting the idea that TA variations in this data set result only from the mixing between AW and sea ice meltwater.

Biological processes like organic matter photosynthesis/respiration (P/R) and calcification/carbonate dissolution (NCC) are expected to influence slightly TA concentration (Middelburg et al., 2020). In order to better understand the importance of these biological processes in the TA distribution, the differences between two end-members mixing line and the measured TA values (Figure 5) were calculated (ΔTA_{bio}) (see methods). Therefore, TA_{bio} represents the changes in TA which are not due to the mixing of AW with melted sea ice.

The average [± standard deviation (SD)] of ΔTA_{bio} for 2019 is 10.0 ± 8.5 μmol kg^{-1} (Figure 5). Data collected during 2020 also shows a positive shift ΔTA_{bio} of 4.2 μmol kg^{-1} (SD ± 9.9 μmol kg^{-1}). On the other hand, in 2021, the TA measured was the closest to the ideal mixing line (TA_{sal}), with a ΔTA_{bio} of 0.7 μmol kg^{-1}, SD ± 8.8 μmol kg^{-1}.

As for TA, the conservative mixing line (DIC_{sal}) formed by linking values for winter AW (salinity 34.96 and DIC_{wv} = 2160 μmol kg^{-1}, Table 1) and melted sea ice water (salinity 5.3 and DIC_{ice} =369 μmol kg^{-1}) is represented as a black line in Figure 5. The deviations from this line are caused due to other mechanisms besides the physical mixing of AW and sea ice meltwaters, namely

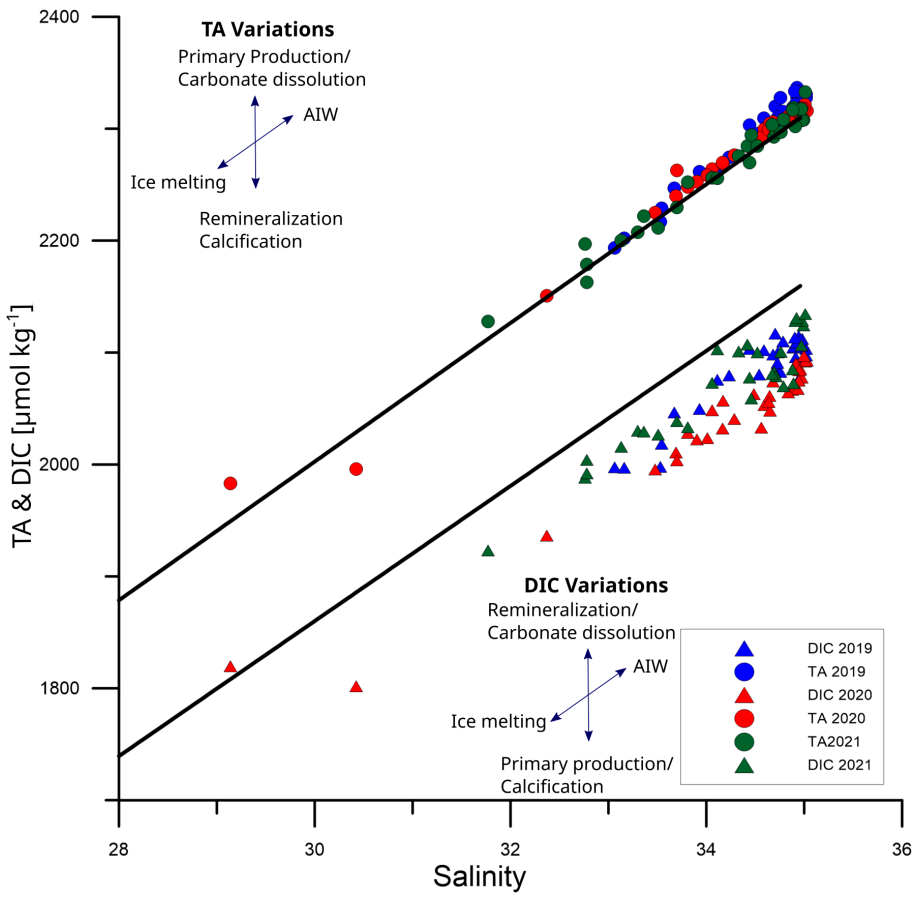

FIGURE 5
Concentration of TA and DIC against salinity. The black line represents the conservative mixing between Atlantic Water encountered in the study area during winter and melting sea ice. Triangles show DIC concentration, while circles are for TA. Data with blue colour were collected during July 2019, red during July 2020, and green during July 2021. Arrows represent the direction of change from the equilibrium due to different processes. Air-sea fluxes are not represented, but they change DIC concentration in the same direction as Remineralization and Primary Production.

organic matter photosynthesis/respiration, calcification/carbonate dissolution and CO_2 air-sea exchange (ΔDIC_{bio}).

All measured DIC values, ranging from 1800 to 2120 µmol kg^{-1}, were below this line and revealed variability higher than for ΔTA_{bio}. DIC data presented here have a wider range than previously recorded at 6m water depth for this area by Tynan et al. (2016) (from 2040 to 2120 µmol $kg^{-1)}$ and the data collected within the first 6m of the water column by Chierici et al. (2019) (from 1883 to 2084 µmol kg-1). This may indicate that, due to the high stratification in the surface waters, a shallower sampling depth (2.5m in this study) resulted in a wider range of DIC data. Therefore, the sampling depth should be taken into consideration, especially when estimating air-sea carbon fluxes. The mean ΔDIC_{bio} for 2019, 2020, and 2021 were -50.0, -73.4, and -42.9 µmol kg^{-1}, respectively (SD ±12.7 µmol kg^{-1} for 2019; SD ±18.7 µmol kg^{-1} for 2020; and, SD ±18.8 µmol kg^{-1}).

Both NCC and P/R modify DIC and TA in given proportions. P/R decreases approximately 6.3 moles of DIC for each 1 mol of TA increase, while NCC decreases DIC and TA in the molar proportion of 1:2 (e.g., Middelburg et al., 2020). However, the DIC concentrations, opposite to TA, are further modified by the air-sea CO_2 fluxes. Since the surface waters in Fram Strait were undersaturated in CO_2 with respect to the atmosphere (this study), the air-sea CO_2 fluxes always led to an increase in DIC concentration.

A positive ΔTA_{bio} (10.0 µmol kg^{-1}) and a negative ΔDIC_{bio} (-50.0 µmol kg^{-1}) were obtained for 2019. In previous studies P/R has been identified as the main factor influencing the marine carbonate system in the Fram Strait area (Chierici et al., 2019) and the adjacent Barents Sea (Fransson et al., 2001). Assuming that P/R is the primary process influencing also our data, the ΔTA_{bio} of 10.0 µmol kg^{-1} for 2019 should correspond to ΔDIC of -63 µmol kg^{-1}, which is a more significant decrease in DIC than the ΔDIC calculated in our study (-50.0 µmol kg^{-1}). This difference could be due to an uptake of atmospheric CO_2 increasing the DIC of the surface waters.

Using the same assumption of P/R as the most important process, the ΔTA_{bio} of 4,2 µmol kg^{-1} found for 2020 would correspond to -26.1 DIC µmol kg^{-1}, which is a much smaller DIC loss than the observed ΔDIC_{bio} (-73.4 µmol kg^{-1}). However, calcite formation during coccolithophorid blooms is a common phenomenon in the mixing zone of Atlantic and Arctic waters (PSWw) (Lalande et al., 2011), and this process counteracts the TA release by P/R. Thus, the contribution of biological calcium carbonate export from surface waters would explain the low

ΔTA_{bio} encountered for 2020 as compared to the highly negative values of ΔDIC_{bio}.

A similar pattern as for 2020 can be described for 2021, for which P/R alone cannot explain the DIC loss (ΔDIC_{bio} = -42.9 µmol kg^{-1}) based on ΔTA_{bio} (0.7 µmol kg^{-1}). The smallest DIC loss in 2021 (the lowest absolute ΔDIC_{bio} value compared to 2019 and 2020) may indicate a lower P/R that year and, in combination with low ΔTA_{bio}, may suggest a shift in the biological community towards the increase in the relative abundance of calcifying organisms. While diatoms have been reported as the dominant species in cold and nutrient-rich waters close to the sea ice front, coccolithophores are more abundant, particularly during summer, in the eastern ice-free part of Fram Strait (Lalande et al., 2013; Nöthig et al., 2015). In southern warmer areas, both of them are often replaced by nano- and picoplankton (Bauerfeind et al., 2009; Nöthig et al., 2015), which is related to faster nutrient recycling and lower carbon export (Forest et al., 2010). 2019 was characterized by warmer waters than 2021 and a farther northern extension of the surface AW signature, together with positive ΔTA_{bio} (10.0 µmol kg^{-1}) and a negative ΔDIC_{bio} (-50.0 µmol kg^{-1}). As a result, the ratio between nano-picoplankton and calcifiers as the main drivers for PP is expected to be higher during the warmer 2019 than during the colder 2021, characterized by much smaller ΔTA_{bio} (0.7 µmol kg^{-1}) but similar (ΔDIC_{bio} = -42.9 µmol kg^{-1}) as 2019.

Thus, the interannual shifts in dominating species can be proposed as an explanation for the variable ratios between ΔTA_{bio} and ΔDIC_{bio} in different years, when either the proximity of the sea ice front changes with respect to the study area (diatoms vs. coccolithophorids) or there are differences in seawater temperature (coccolithophorids vs. nano- and picoplankton species).

To sum up, the ratio between $\Delta DIC_{bio}/\Delta TA_{bio}$ suggests that during the warmer 2019 and 2020, there was a higher P/R in the area (this assumption is further supported by satellite chlorophyll data in the next section) than during the colder 2021. Besides that, it also indicates a shift in the ratio between calcifiers and nano-picoplankton, where warmer years could promote a reduction of calcifiers with respect to nano-picoplankton.

The changes in DIC and TA presented in this section are strongly connected to changes in pCO_2 and pH. Both of them play a key role as indicators of atmospheric carbon sequestration and ocean acidification. Due to the sampling strategy, pH and pCO_2 data were collected in higher resolution, providing not only information about their general distribution but also about mesoscale processes which could influence their variability.

3.2.2 Surface pCO_2

The pCO_2 measurements in all investigated years (2019-2021), with average values of 288, 271 and 286 µatm for 2019, 2020 and 2021, respectively, show that the entire study area was undersaturated with CO_2 relative to atmospheric levels which were, in annual average, 412, 414 and 417 ppm (data obtained from environmental monitoring of Svalbard and Jan Mayen; https://mosj.no), which is in agreement with other studies in Fram Strait and around Svalbard (e.g., Chierici et al., 2019; Fransson et al., 2017; Tynan et al., 2016; Yasunaka et al., 2018);. The pCO_2 values ranged from 170 µatm found near the sea-ice edge and were associated with the presence of colder, lower salinity waters, up to 350 µatm observed in the southern part under the influence of warmer and more saline Atlantic waters (Figure 6). The distribution of surface pCO_2 (Figure 6) shows a similar pattern as salinity (Figure 3A), with values decreasing from South to North and the highest values centred at approximately 10°E (similar to the AW surface patch area). The surface pCO_2 rapidly declined as we moved closer to the continental margin of Svalbard and the sea-ice edge.

In general, lower values of pCO_2 were found within the AW surface patch in 2020 (average pCO_2 303 µatm) than in 2021 (average pcO_2 329 µatm), while similar values have been found outside of this area (approx. 255 µatm). The lower pCO_2 in 2020 coincided with the lowest DIC concentrations found in our study, which could reflect higher P/R in the area that year (Figure 6). Figure 7 shows the monthly averaged distribution of chlorophyll *a* estimated from satellite observations (NASA Ocean Biology Processing Group, 2023). Higher chlorophyll *a* concentration are visible within the AW surface patch (10°E) in 2020 (average chlorophyll *a* in AW surface patch area of 1.14 mg m^{-3}) than in 2021(average chlorophyll *a* 0.82 mg m^{-3}), while in 2021, the maximum of PP (highest chlorophyll *a*) was located further west of the AW inflow area.

In 2019, the chlorophyll *a* distribution (average in the study area of 3.00 mg m^{-3}) was higher to that in 2020 (chlorophyll *a* 1.05 mg m^{-3}), with higher PP within the AW inflow (average of 2.21 mg m^{-3}). This feature is, however, not reflected so clearly in the DIC and pCO_2 – both being higher in 2019 (DIC_{bio} -50.0 µmol kg^{-1} and average pCO_2 289 µatm) than in 2020 (DIC_{bio} -73.4 µmol kg^{-1} and average pCO_2 271 µatm). The reason for that and the coinciding smaller DIC loss (lower absolute value of ΔDIC_{bio}) and relatively high accumulation of TA (reflected with ΔTA_{bio}) measured during 2019 could be related to a delay between the sampling time and the peak of high PP. The satellite images represent the monthly averaged chlorophyll *a* distribution while pCO_2 (as well as TA and DIC) was collected within days, which may generate a mismatch between both datasets.

To sum up, the lower pCO_2 was correlated with lower salinity waters. Areas influenced by AW (salinity greater than 34.8) had a strong interannual variability: during the investigated period we can distinguish between two years (2019 and 2020) characterized by a high signal of PP within the AW surface patch and, one year (2021) with low PP within the study area but high PP westward of the AW inflow (outside of the study area and only based on satellite data).

The pCO_2 data not only shows a general south-to-north gradient (Figure 6), but it is possible to recognize rapid and small/medium scale latitudinal and longitudinal changes of pCO_2 due to the higher resolution data. To depict them and understand the mechanism behind these variations, three surface pCO_2 transects from 2021 (a year for which both the south-to-north pCO_2 variability and pCO_2 data coverage were high) were selected and plotted in Figure 8:

- southern profile (76° N), with higher values of pCO_2 (between 270 µatm and 340 µatm) coinciding with high salinity.

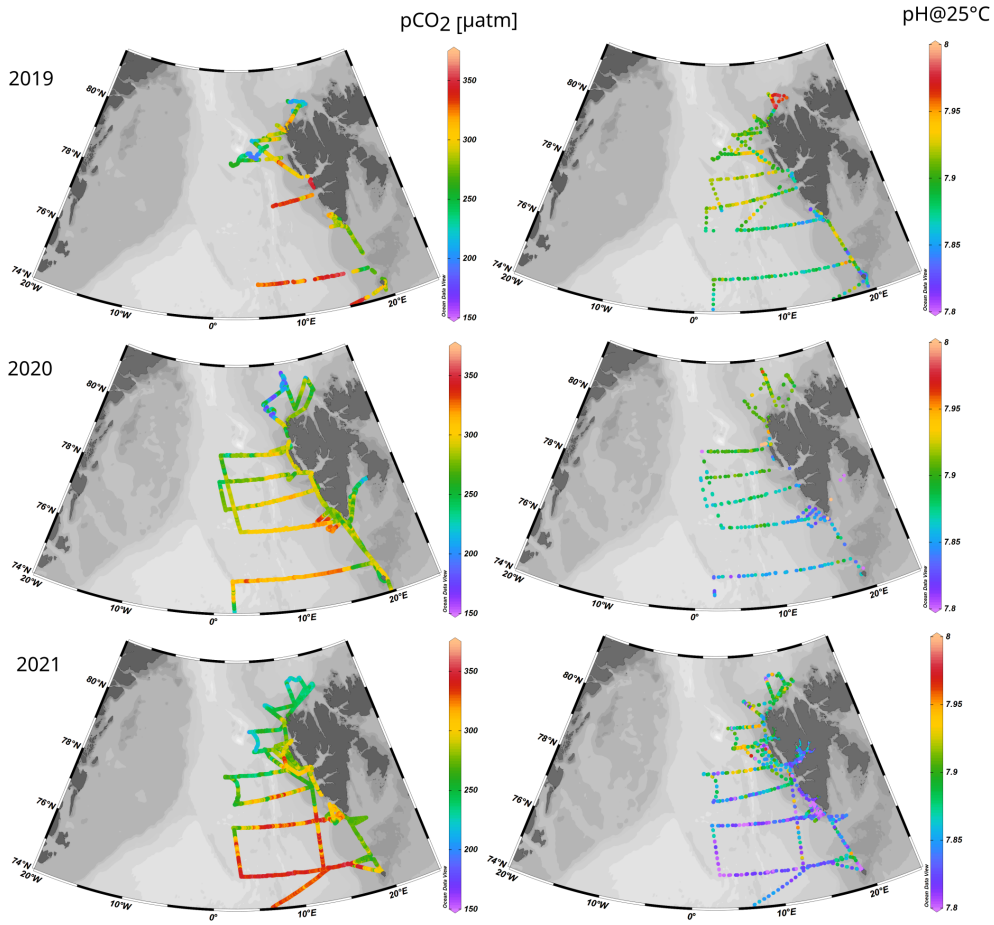

FIGURE 6
Surface distribution of pCO_2 (left) and pH at 25°C (right) from 2019 (top), 2020 (middle) and 2021 (bottom).

- middle profile (77° N), with strong spatial variations of surface pCO_2 (ranging between 240 µatm and 310 µatm), salinity, and temperature.
- northern profile (79° N), with significantly lower values of pCO_2 (from 230 µatm to 250 µatm) and a drastic latitudinal reduction of salinity due to the proximity of the sea ice.

The variability in pCO_2 along the latitudinal transects can be influenced by several factors: temperature, salinity (or mixing of different water masses), P/R, and upwelling of deeper waters with different pCO_2. To simplify the interpretation of this variability, the pCO_2 data was normalized to 5°C ($NpCO_2$) using the temperature dependence proposed by Takahashi et al. (2002). The $NpCO_2$ was plotted in Figures 8A–C with oxygen data as a proxy for P/R, and with salinity to understand the pCO_2 changes due to mixing effects.

In the southernmost transect (Figure 8C), two main features related to variations in pCO_2 can be recognized. First, there was a salinity reduction, a slight increase in the O_2 saturation, and a decrease in pCO_2 west of 5°E, probably related to the influence of PSWw along the GSG. The second feature was a correlation between the O_2 saturation and the pCO_2 but without large changes in salinity east of 5°E, indicating variability in P/R only. The increases in P/R without salinity changes could be due to the vertical transport of deeper water (e.g. from the chlorophyll maximum depth) to the surface. Theoretically, the mechanism explaining it could be the influence of eddy-driven upwelling or wind-driven increase in the mixed layer depth, which could bring a signal of higher P/R from deeper waters to the surface.

In the middle transect (Figure 8B), several areas with salinity drop can be identified. One is located between 2°E and 3°E and reflects the influence of PSWw, but with minor changes in oxygen and pCO_2. A second patch with a strong drop in salinity of 1 unit was located at 6.5°E, followed by an oversaturation of O_2 up to 108 µmol kg^{-1} and an intense reduction of pCO_2 by more than 50 µatm. The reason for this salinity drop was probably an intrusion of a filament of PSWw in the surface layer occupied by AW. The different O_2 and pCO_2 dynamics, thus also different P/R, observed for these two salinity perturbations could be related to nutrient availability. Previous studies showed that surface waters of Arctic origin are generally nitrate-limited, while AW is mostly Fe-limited (Krisch et al., 2020; Tuerena et al., 2021). The injection of PSWw into the mainstream of AW may cause a mixture of water masses, providing extra nitrate from AW to PSWw and Fe from PSWw to AW and inducing an intense P/R. This feature was well seen at 6.5°E but not at 3°E, maybe because the latter region does not represent a PSWw intrusion into AW (and mixing of both) but

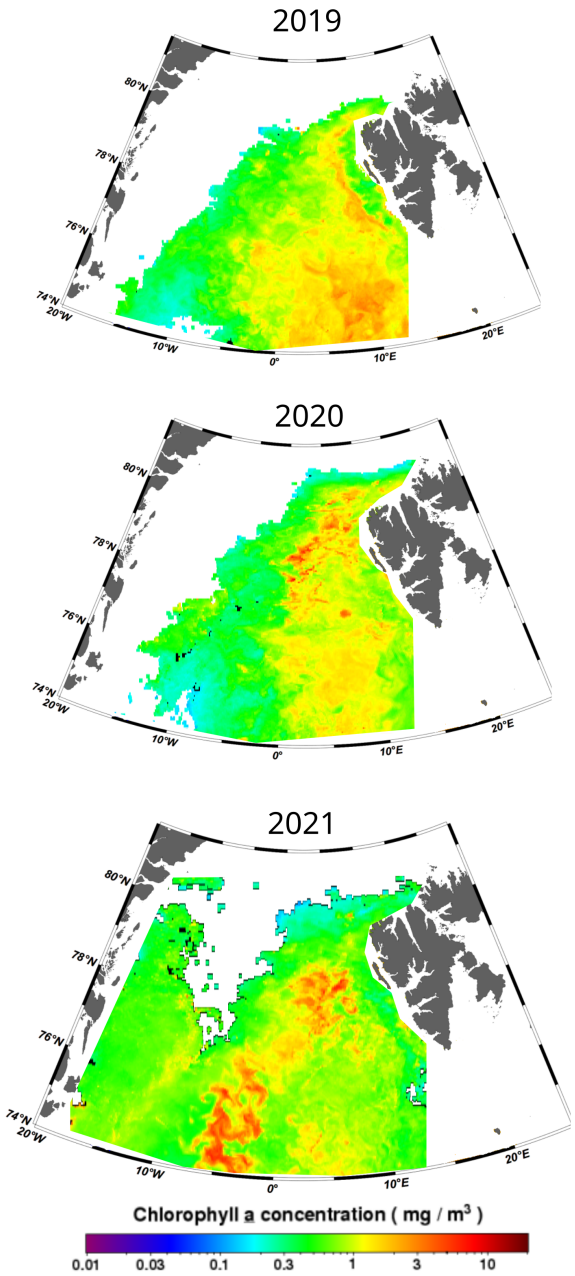

FIGURE 7
Satellite-derived MODIS-Aqua monthly average composite chlorophyll *a* concentration (mg/m^3) for July 2019, 2020, and 2021 (NASA Ocean Biology Processing Group., 2023).

rather the boundary between PSWw and AW with clear separation of both water masses properties. Still, an increase in O_2 saturation on the edge of the salinity drop (between 3°E and 4°E) is distinguishable and probably related to the mixing of PSWw and AW. Along the middle transect (Figure 8B), there was one more area with a salinity drop located east of 11.5°E and associated with an increase in O_2 saturation and a decrease in pCO_2, probably due to both the dilution effect and the P/R. In this case, it was connected to the influence of meltwater released from the Spitsbergen fjords and/or the influence of the South Cape Current that propagates northward along the west coasts of Spitsbergen. Interestingly, along the same latitude (Figure 8B) there was an area from 7.5°E to 11.5°E where the salinity remained constant, but the pCO_2 was highly variable and coupled with the O_2 saturation (the relationship between ΔpCO_2 and O_2 saturation is provided as Supplementary Material, Supplementary Figure S2). As postulated above, the eddy-driven upwelling of deeper waters (or the deepening of the mixed layer) from the maximum chlorophyll depth (typically located at 20-30m water depth) carrying a higher P/R signal, could explain this rapid phenomenon, although future studies correlating the variability of pCO_2 and O_2 in surface layers with changes in the mixed layer depth are needed to support this theory.

The northernmost transect (Figure 8A) was highly influenced by continental runoff, and sea-ice melted water.

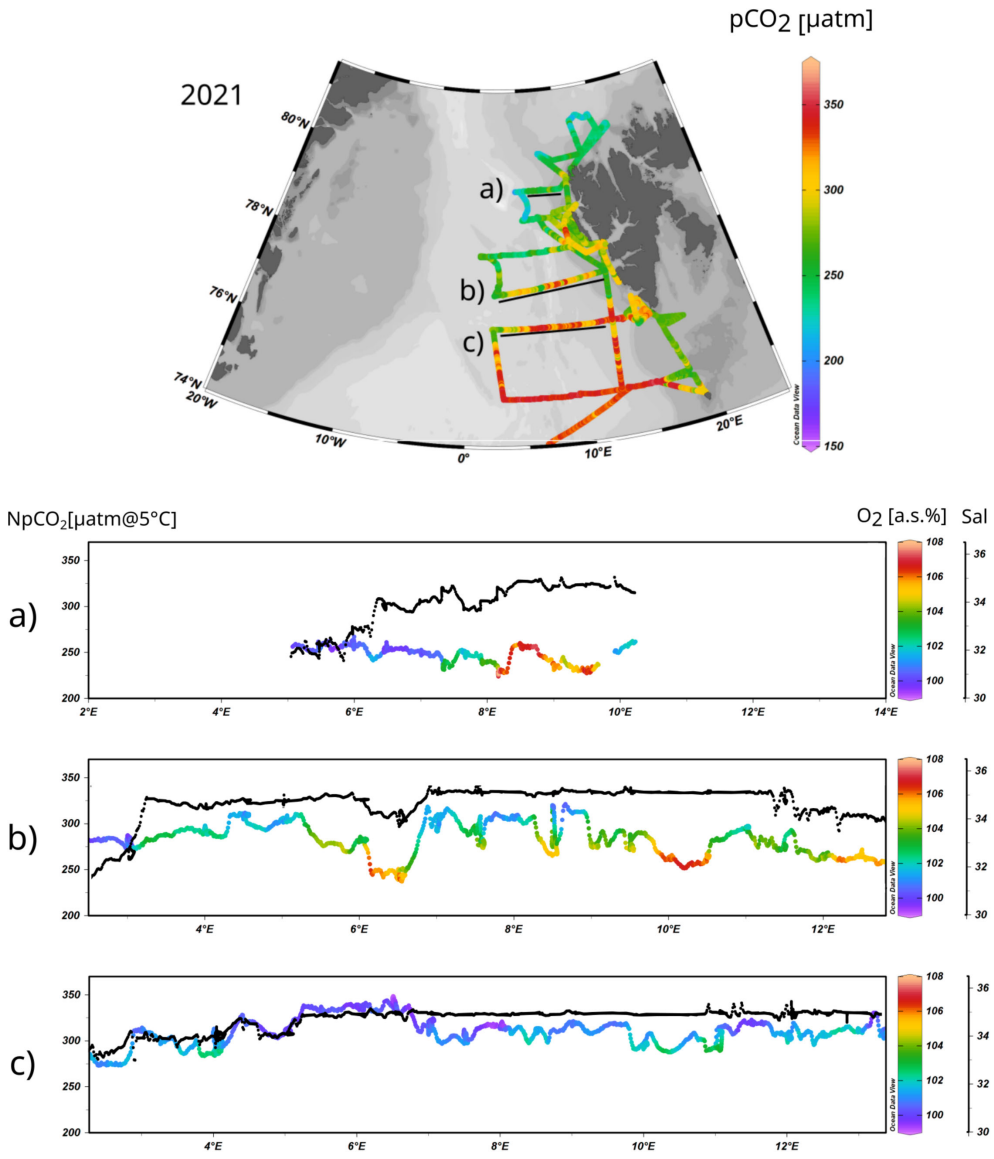

FIGURE 8
Surface distribution of pCO_2 (top) during the sampling campaign in 2021. The transects **(A–C)** marked in the surface pCO_2 distribution map are displayed at the bottom of the figure. The black line within the transects shows salinity variations, the colourful line represents $NpCO_2$ (normalized pCO_2 to 5°C), and the colour scale within the colourful line depicts O_2 (a.s.). All the transects display data collected during 2021.

From 5°E to 7°E, the dilution effect (salinity drop by approx. two units) maintained undersaturated levels of pCO_2 (250 µatm) with O_2 being close to the equilibrium with the atmosphere. East of 8°E, similarly low pCO_2 (250 µatm) was measured. However, in this case, it was a consequence of the intense P/R, indicated by an oversaturation in the water O_2 with respect to the atmospheric levels (up to 108%).

Altogether, four processes have been identified that potentially contribute to pCO_2 reduction in the studied region and thus enhance the water capacity to absorb atmospheric CO_2. These are: (1) the dilution effect due to PSWw's influence, (2) the P/R increase due to the mixing of nutrient pools of AW and PSWw, (3) wind-driven increase in the mixed layer bringing higher P/R signal from deeper waters, (4) the influence of lower salinity waters in the western coast of Spitsbergen.

3.2.3 Surface pH distribution

Along with temperature, salinity, and pCO_2, the pH distribution was affected by an intense latitudinal variation with lower pH values observed in the southern part associated with warmer waters having higher pCO_2, and higher pH values measured close to the sea ice and the continental margin (Figure 6). Importantly, pH was measured at 25°C; therefore, the distribution of pH presented in this study is not influenced by temperature variations, in contrast to pCO_2 distribution. Comparing the three consecutive years of investigations, 2021 had the lowest pH value (7.8), increasing up to 7.95 in the northern part; 2019 had the highest pH, ranging from 7.85 to 8.1, while in 2020, pH values were intermediate and ranged from 7.85 to 8.0.

Since inorganic carbon chemistry heavily influences the pH, it is expected that the processes triggering changes in pCO_2 can also be

traceable in the pH distribution (excluding temperature). Still, if the general trends in pH and other CO_2 system variables are compared within the area of AW surface expression, it can be concluded that higher values of pCO_2 were found in 2019 and 2021 than in 2020 (Figure 6). Both years (2019 and 2021) also had similar DIC concentrations, higher than in 2020 (Figure 5). However, this situation is not reflected in pH (Figure 6), where 2019 had higher values coinciding with the higher values of TA (Figure 5), followed up by 2020 and 2021, which had lower pH and lower TA. As postulated above, it could be due to a change in the characteristics of the plankton community, increasing the abundance of calcifying organisms in years with colder and fresher surface waters and consequently reduced alkalinity of surface waters, making them more sensitive to pH changes. Therefore, not only the pCO_2 distribution is important for understanding the pH variability in the Fram Strait area, but it is also essential to know the distribution of TA and biologically driven ΔTA_{bio}.

To better understand the pH variations in the region due to different physical and biological factors, their influences have been quantified, as described in section 2.2, and presented in Figure 9. The range of the temperature effect on pH (ΔpH_{temp}) is from a reduction of -0.08 in the warmer and more saline waters to an increase of 0.06 close to the sea ice (values represent the minimum and maximum from all the years). Importantly, these changes in pH due to temperature variations refer to a semi-arbitrary reference point ($Temp_{wv}$) established for winter conditions (see methods). Thus, the ΔpH values do not provide any valuable information other than the absolute difference between maximum and minimum. This difference reflects the variability in pH due to the temperature gradient between the warmer and colder waters in the region. As a result, the ΔpH_{temp} due to the temperature factor is approx. 0.14 and can be understood as the pH change due to the cooling of waters as they flow northwards. The effect of dilution (or seawater freshening) is defined as ΔpH_{sal} and is responsible for a pH increase in the region of approx. 0.1, with a wide range of ΔpH_{sal} values from 0.01 to 0.10 being inversely correlated with salinity. The ΔpH_{bio} is the integrated effect of the P/R, NCC, and air-sea fluxes. Its average values varied widely from year to year, with an average of 0.18, 0.22, and 0.10 for 2019, 2020 and 2021, respectively. Additionally, the consistency of the marine CO_2 system variables was presented as pH_{inc} as an expression of the variability in the data due to uncertainties derived from calculations and the propagation of errors during the analytical measurements. The average of pH_{inc} was 0.02 which is much lower than ΔpH_{bio} but also than ΔpH_{temp} or ΔpH_{sal}, suggesting that even though there are some uncertainties related to the calculations with the use of CO2SYS, they are usually lower than the effect of any of the factors influencing pH variability. Still, the effect of the inconsistencies in the marine CO_2 system should not be ignored in pH-oriented studies in this region, as depending on the scope of conducted research they may constitute an important source of uncertainty.

The results clearly show that ΔpH_{bio} is the main factor controlling the pH distribution in Fram Strait surface waters. Interestingly, the two years with greater ice extension (2019 and

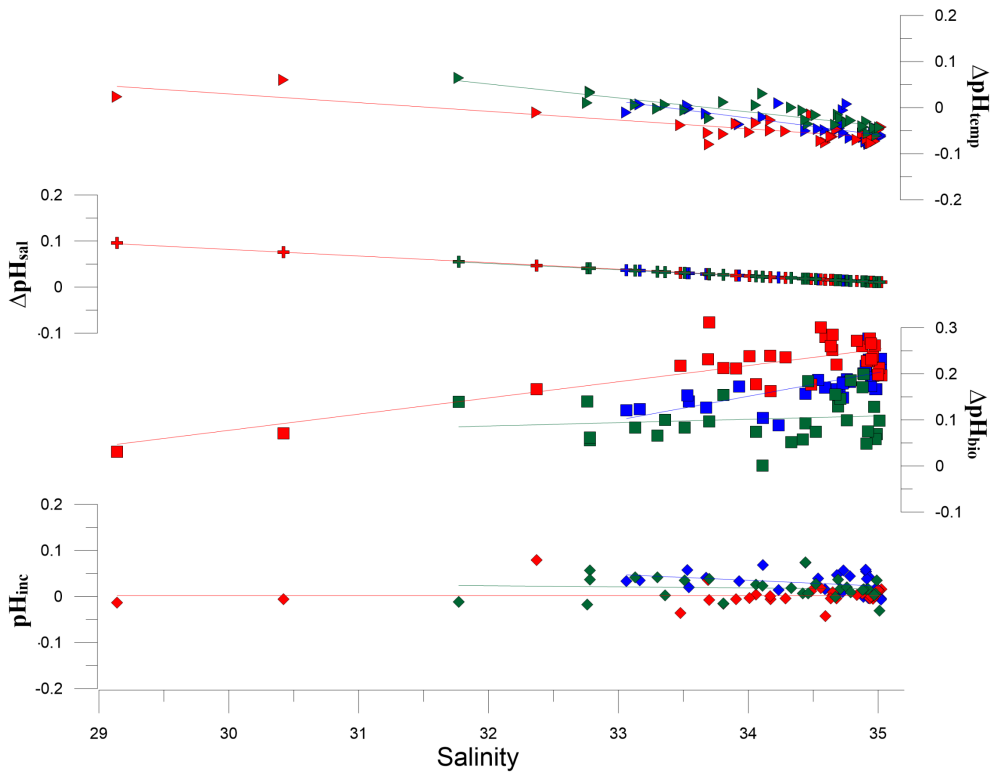

FIGURE 9
Correlation between different ΔpH (associated with temperature ΔpH_{temp}, salinity ΔpH_{sal}, the combined effect of NPP, NCC, and air-sea fluxes ΔpH_{bio}, and inconsistencies pH_{inc}) and salinity. Blue dots are data from 2019, red dots from 2020, and green dots from 2021.

2020) were also characterized by higher pH variation due to ΔpH_{bio}. It is also worth mentioning that the influence of dilution close to the sea ice margin can be similar in magnitude to the pH change due to the temperature variations, both creating rapid pH fluctuations and directly influencing the CO_2 system structure. Thus, with their combined effects, sea ice melting and temperature variability are unneglectable drivers affecting the distribution of surface pH in the eastern Fram Strait, which must be considered for investigating ocean acidification development under future climate scenarios.

3.3 Synthesis

Overall, 2019 and 2020 were characterized by warmer surface waters with a northern extension of the surface AW patch (seawater with salinity greater than 34.8), coincidentally with a broader sea ice extension. On the other hand, 2021 had colder waters, and the surface extent of AW was reduced in the study area, coinciding with the smaller sea ice extension. The mechanism to explain the temperature and salinity variability could be an increase in the PSWw influence on the area and/or a reduced surface expression of AW in years with enhanced sea ice melting due to the higher admixture of meltwater.

The results from DIC and TA indicate that it was possible to trace higher P/R in the AW-influenced area during warmer years (2019 and 2020), coinciding with a lower presence or abundance of calcifier organisms as suggested by the ratio $\Delta TA_{bio}/\Delta DIC_{bio}$. Furthermore, these results coincide with the distribution of surface pCO_2 and pH, where warmer years with higher P/R have also lower pCO_2 at the surface and higher pH, intensifying the capacity of the surface waters to absorb atmospheric CO_2, even though warmer surface waters have reduced CO_2 solubility. Satellite images of chlorophyll *a* distribution also support the idea of higher P/R within the eastern Fram Strait during warmer years. Our conclusions agree with previous findings which suggest that warmer waters may sustain the pycnocline in the surface layer for longer periods, favouring the development of primary producers (Cherkasheva et al., 2014).

Besides the general trends, the high-resolution data of pCO_2 indicate that other medium/small-scale processes may contribute to rapid changes in surface pCO_2. Several studies have shown the presence of mesoscale/submesoscale eddies in the region (Bashmachnikov, 2020; Ghaffari et al., 2018; Trodahl and Isachsen, 2018), which are especially abundant at the outer boundary of the AW inflow. These features can be likely identified in our dataset as local drops in the surface pCO_2 in the AW frontal zone, which may indicate an upwelling of nutrient-rich waters, enhancing P/R in the surface layers, and/or an upwelling of already low pCO_2 waters related to subsurface production, probably at the bottom of the surface mixed layer (Tuerena et al., 2021).

Our data also shows an intense decrease in surface pCO_2 (and an increase in O_2 saturation) in areas where PSWw meets AW. These areas are characterized by an intrusion of cold waters into the warmer layer, indicating that mixing of PSWw and AW in some sectors may enhance P/R. The differences in nutrient limitation between Arctic and Atlantic-derived surface waters have been previously postulated (Krisch et al., 2020; Tuerena et al., 2021), bringing the idea that the mixing between nitrate-limited Arctic-derived waters (in this study, sea-ice-derived meltwater), and Fe-limited Atlantic-derived waters could create the ideal "nutrient-soup" to enhance P/R.

But this initial enhancement of P/R due to the mixing of water masses could create also a negative effect, as seen in 2021, where chlorophyll data shows that the intense PP area was moved westward. Therefore, the reduction of sea ice would move the PP westward, and, an expansion of PSWw (already depleted in nitrates) could create a colder nitrate-limited surface layer, which will produce, as observed in 2021 higher DIC and pCO_2 in the surface layer. These waters may intensify the seasonal pycnocline, deepening it or reducing the eddy-driven upwellings. Consequently, years with colder (or rather higher influence of melted sea ice) surface waters may result in reduced P/R in the eastern part of the Fram Strait.

The mechanism to explain how a higher volume of PSWw may influence the study area is not clear and cannot be fully explained with the data presented in this study. Nevertheless, it can be hypothesised that due to the direct mixing or by the influence of the GSG, more meltwater is incorporated within the surface waters of the eastern part of Fram Strait. With this idea in mind, and based on our biogeochemical data, Figure 10 shows a theoretical concept connecting the main factors influencing the carbonate system in the eastern Fram Strait in two hypothetical scenarios: the first one with a lower influence of melted sea ice waters and lower extension of PSWw within the WSC (Figure 10A) and the second one with a wider extension of PSWw due to higher volume of sea ice meltwater (Figure 10B).

In the scenario with a lower influence of melted sea ice waters (Figure 10A), there is a high P/R in the eastern Fram Strait, which is likely associated with larger vertical nutrient fluxes linked to more abundant mesoscale eddies. Alternatively, the intrusion of PSWw in the surface layer occupied by AW may also enhance P/R by mixing waters with different nutrient limitations. Consequently, enhanced P/R, a higher abundance of nano-pico plankton, and a reduced influence of calcifiers would result in elevated alkalinity and enhanced capacity to capture anthropogenic CO_2 in surface waters.

In the high PSWw scenario and a strong influence of sea ice meltwater on the surface layers, P/R is concentrated close to the sea ice margin zone, which acts as a nutrient filter, depleting their concentrations. The link between sea ice extension and phytoplankton distribution during spring and summer was proposed by Mayot et al. (2020), showing that in years with low export of sea ice, a late-spring/summer phytoplankton bloom develops close to the sea ice margin. These nutrient-depleted waters may follow the surface currents following the EGC, which could expand eastwards the area influenced by PSWw, initially enhancing P/R in a southern location (GSG) but have a low capacity to sustain high primary production in the study area (eastern Fram Strait). This is probably due to the stratification of fresher and colder waters at the surface with an unknown effect on the eddy-driven circulation and the upwelling of deeper N-rich waters.

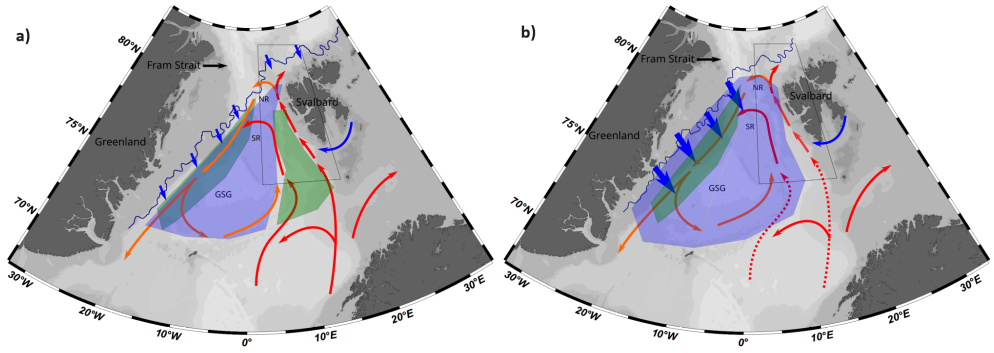

FIGURE 10
Theoretical concepts of the biological and physical situation in the area during: **(A)** narrower extension of warm Polar Surface Waters (PSWw) connected to a lower volume of sea ice meltwater (small blue arrows) in the surface layer and, **(B)** broader extension of PSWw as a consequence of a higher volume of sea ice meltwater in the surface layer. The blue area represents the zones of intense influence of PSWw, and the green area stands for the intense NPP zones developed during summer. The colour in the arrows represents a schematic view of the main water masses in the area and their transformations. Blue arrows represent the influence of Arctic waters, either as melted sea ice (small ones), or as Arctic waters carried by the South Cape Current (SCC), located south of the Svalbard Archipelago. The red arrows represent the Atlantic Water (AW), and the orange arrows are the Polar warm Surface Waters (PSWw). GSG, NR, and SR denote Greenland Sea Gyre, Northern Recirculation, and Southern Recirculation, respectively. The blue line represents the 10% sea ice coverage (SIC), northern of this line the SIC is higher than 10%.The black box delimits the study area.

Stratified waters with lower P/R would limit the capacity of the surface waters to capture atmospheric CO_2. This hypothesis implies that the influence of the sea ice meltwater within the Fram Strait is crucial for estimating and understanding the capacity of the region to absorb atmospheric CO_2. Future scenarios project a reduction in Arctic sea ice during summer. However, a better understanding of the relationship between the volume of melted sea ice and the biogeochemical processes in the surface waters is required, not only in the Fram Strait area but also in the Arctic Ocean in general.

4 Conclusions

This study investigated the distribution of the marine carbonate system parameters, as well as salinity and temperature in consecutive summers of 2019, 2020, and 2021 in the surface waters of the eastern part of the Fram Strait. This, together with analysis of the satellite-derived chlorophyll *a* distribution as well as sea ice extension in the region allowed us to draw the following conclusions:

- TA and DIC are mostly controlled by the mixing of Atlantic water and sea ice meltwater. The combined effect of organic matter production/remineralization, calcium carbonate precipitation/dissolution, and air/sea CO_2 gas exchange causes deviations from this salinity-related mixing, which are smaller and positive for TA (ΔTA_{bio} from 0.7 to 10.0 µmol kg^{-1}) and larger and negative for DIC (ΔDIC_{bio} from -42.9 to -73.4 µmol kg^{-1}).
- The ratios between ΔTA_{bio} and ΔDIC_{bio} suggest interannual shifts in P/R and dominant phytoplankton species in the area. The results indicated higher productivity (confirmed by satellite-derived chlorophyll *a* as well as pCO_2 and pH distribution) and a lower proportion of calcifying to non-calcifying species during 2019 and 2020 characterized by higher surface water temperatures compared to the colder year 2021.
- Net primary production is the main factor controlling the temporal and spatial variability of pH and pCO_2 in the study area followed by temperature (effects of seasonality and cooling as the Atlantic Waters propagate northward) and mixing of water masses expressed with salinity (seawater freshening).
- The patchiness in the latitudinal and longitudinal distributions of pCO_2 and O_2 saturation and their irregular relationship with salinity suggest that vertical mixing of the water column as an important process in shaping surface pCO_2 fields and P/R in the Fram Strait area.
- There is a need to better understand the role of sea ice extent and the associated spread of warm Polar Surface Waters (mixture of Polar Waters and Atlantic Waters) in controlling primary production in the region, which is crucial for predicting the capacity of Fram Strait waters for absorbing atmospheric CO_2 in the future with less sea ice. The smaller sea ice extent and greater spread of warm Polar Surface Waters observed in 2021 coincided with a westward shift of the chlorophyll *a* maximum towards the sea ice front. A reverse situation was observed in 2019 and 2020, when greater extension of Atlantic Waters in the eastern part, as well as sea ice in the western part of the Fram Strait area, were accompanied by chlorophyll *a* maximum in the Atlantic Waters.

Data availability statement

The datasets presented in this study can be found in online repositories. The names of the repository/repositories and accession number(s) can be found below: https://doi.org/10.48457/iopan-2024-159.

Author contributions

FG: Conceptualization, Writing – review & editing, Data curation, Formal analysis, Investigation, Methodology, Visualization, Writing – original draft. MS: Data curation, Methodology, Writing – review & editing. KK-M: Data curation, Writing – review & editing. PM: Data curation, Writing – review & editing. AB-M: Data curation, Writing – review & editing. PK: Conceptualization, Funding acquisition, Writing – review & editing. KK: Conceptualization, Funding acquisition, Project administration, Supervision, Validation, Writing – review & editing.

Funding

The author(s) declare financial support was received for the research, authorship, and/or publication of this article. Sampling, chemical analyses, and data interpretation related to the marine CO_2 system structure and variability were financially supported by the Polish National Science Center, grant no. 2019/34/E/ST10/00167, under the project PROSPECTOR. The analysis of the interrelationships between sea ice extent and chlorophyll *a* distribution was supported by the European Union within the Horizon Europe programme, project 101136480 — SEA-Quester. The interpretation of the seawater freshening was supported by the Norwegian Financial Mechanism 2014–2021 (85%) and National Science Centre (15%) within the GRIEG Programme, grants no. 2019/34/H/ST10/00504 and 2019/34/H/ST10/00645. Additionally, the contribution of PK to the study was supported by the Polish National Science Center, grant no. 2020/37/B/ST10/02905.

Acknowledgments

We would like to thank HEREON for allowing KK-M to measure DIC and TA samples collected in 2020 and also to OBPG/OB.DAAC for providing public access to Satellite Chlorophyll data included in this manuscript. We also would like to thank the captain and the crew of the R.V. Oceania for their enthusiasm and support during sampling.

Conflict of interest

The authors declare that the research was conducted in the absence of any commercial or financial relationships that could be construed as a potential conflict of interest.

Publisher's note

Supplementary material

The Supplementary Material for this article can be found online at: https://www.frontiersin.org/articles/10.3389/fmars.2024.1464653/full#supplementary-material

References

Ahmed, M. M., Else, B. G., Capelle, D., Miller, L. A., and Papakyriakou, T. (2020). Underestimation of surface pCO2 and air-sea CO2 fluxes due to freshwater stratification in an Arctic shelf sea, Hudson Bay. *Elementa* 8 (1), 084. doi: 10.1525/elementa.084

Arrigo, K. R., and van Dijken, G. L. (2015). Continued increases in Arctic Ocean primary production. *Prog. Oceanography* 136, 60–70. doi: 10.1016/j.pocean.2015.05.002

Arrigo, K. R., van Dijken, G. L., Castelao, R. M., Luo, H., Rennermalm, Å. K., Tedesco, M., et al. (2017). Melting glaciers stimulate large summer phytoplankton blooms in southwest Greenland waters. *Geophysical Res. Lett.* 44, 6278–6285. doi: 10.1002/2017GL073583

Athanase, M., Provost, C., Pérez-Hernández, M. D., Sennéchael, N., Bertosio, C., Artana, C., et al. (2020). Atlantic water modification North of svalbard in the mercator physical system from 2007 to 2020. *J. Geophysical Research: Oceans* 125, 1–26. doi: 10.1029/2020JC016463

Bashmachnikov, I. L. (2020). Eddies in the North Greenland sea and fram strait from satellite altimetry, SAR and high - resolution model data. *J. Geophysical Research : Oceans* 125 (7), e2019JC015832. doi: 10.1029/2019JC015832

Bashmachnikov, I. L., Raj, R. P., Golubkin, P., and Kozlov, I. E. (2023). Heat transport by mesoscale eddies in the Norwegian and Greenland seas. *J. Geophysical Research: Oceans* 128 (2). doi: 10.1029/2022JC018987

Bates, N. R., and Mathis, J. T. (2009). The Arctic Ocean marine carbon cycle: Evaluation of air-sea CO2 exchanges, ocean acidification impacts and potential feedbacks. *Biogeosciences* 6, 2433–2459. doi: 10.5194/bg-6-2433-2009

Bauerfeind, E., Nöthig, E. M., Beszczynska, A., Fahl, K., Kaleschke, L., Kreker, K., et al. (2009). Particle sedimentation patterns in the eastern Fram Strait during 2000–2005: Results from the Arctic long-term observatory HAUSGARTEN. *Deep Sea Res. Part I: Oceanographic Res. Papers* 56 (9). doi: 10.1016/j.dsr.2009.04.011

Beszczynska-Möller, A., Fahrbach, E., Schauer, U., and Hansen, E. (2012). Variability in Atlantic water temperature and transport at the entrance to the Arctic Ocean 1997–2010. *ICES J. Mar. Sci.* 69, 852–863. doi: 10.1093/icesjms/fss056

Brümmer, B., Müller, G., Affeld, B., Gerdes, R., Karcher, M., and Kauker, F. (2001). Cyclones over Fram Strait: impact on sea ice and variability. *Polar Res.* 20, 147–152. doi: 10.1111/j.1751-8369.2001.tb00050.x

Caldeira, K., and Wickett, M. E. (2003). Anthropogenic carbon and ocean pH. *Nature* 425, 365. doi: 10.1038/425365a

Capelle, D. W., Kuzyk, Z. Z. A., Papakyriakou, T., Guéguen, C., Miller, L. A., and Macdonald, R. W. (2020). Effect of terrestrial organic matter on ocean acidification and CO2 flux in an Arctic shelf sea. *Prog. Oceanography* 185, 102319. doi: 10.1016/j.pocean.2020.102319

Carmack, E. C., Yamamoto-Kawai, M., Haine, T. W., Bacon, S., Bluhm, B. A., Lique, C., et al. (2016). Freshwater and its role in the Arctic Marine System: Sources, disposition, storage, export, and physical and biogeochemical consequences in the Arctic and global oceans. *J. Geophysical Res. G: Biogeosciences* 121, 675–717. doi: 10.1002/2015JG003140

Chatterjee, S., Raj, R. P., Bertino, L., Skagseth, Ø., Ravichandran, M., and Johannessen, O. M. (2018). Role of Greenland sea gyre circulation on Atlantic water temperature variability in the fram strait. *Geophysical Res. Lett.* 45, 8399–8406. doi: 10.1029/2018GL079174

Chen, B., Cai, W. J., and Chen, L. (2015). The marine carbonate system of the Arctic Ocean: Assessment of internal consistency and sampling considerations, summer 2010. *Mar. Chem.* 176, 174–188. doi: 10.1016/j.marchem.2015.09.007

Chierici, M., Vernet, M., Fransson, A., and Børsheim, K. Y. (2019). Net community production and carbon exchange from winter to summer in the Atlantic water inflow to the arctic ocean. *Front. Mar. Sci.* 6. doi: 10.3389/fmars.2019.00528

Chierici, M., and Fransson, A. (2009). Calcium carbonate saturation in the surface water of the Arctic Ocean: Undersaturation in freshwater influenced shelves. *Biogeosciences* 6, 2421–2432. doi: 10.5194/bg-6-2421-2009

Cherkasheva, A., Bracher, A., Melsheimer, C., Köberle, C., Gerdes, R., Nöthig, E. M., et al. (2014). Influence of the physical environment on polar phytoplankton blooms: A case study in the Fram Strait. *J. Mar. Syst.* 132, 196–207. doi: 10.1016/j.jmarsys.2013.11.008

Comiso, J. C., Kwok, R., Martin, S., and Gordon, A. L. (2011). Variability and trends in sea ice extent and ice production in the Ross Sea. *J. Geophysical Research: Oceans* 116, 1–19. doi: 10.1029/2010JC006391

de Steur, L., Hansen, E., Mauritzen, C., Beszczynska-Möller, A., and Fahrbach, E. (2014). Impact of recirculation on the East Greenland Current in Fram Strait: Results from moored current meter measurements between 1997 and 2009. *Deep-Sea Res. Part I: Oceanographic Res. Papers* 92, 26–40. doi: 10.1016/j.dsr.2014.05.018

Devries, T. (2022). The ocean carbon cycle. *Annu. Rev. Environ. Resour.* 47, 317–341. doi: 10.1146/annurev-environ-120920-111307

Dickson, A. G., Wesolowski, D. J., Palmer, D. A., and Mesmer, R. E. (1990). Dissociation constant of bisulfate ion in aqueous sodium chloride solutions to 250° C. *J. Phys. Chem.* 94, 7978–7985. doi: 10.1021/j100383a042

Dickson, A. G., and Millero, F. J. (1987). A comparison of the equilibrium constants for the dissociation of carbonic acid in seawater media. *Deep Sea Res. Part A Oceanographic Res. Papers* 34, 1733–1743. doi: 10.1016/0198-0149(87)90021-5

Dickson, A. G., Sabine, C. L., and Christian, J. R. (Eds.) (2007). *Guide to Best Practices for Ocean CO2 Measurements*, Vol. 3 (PICES Special Publication), 191.

Forest, A., Wassmann, P., Slagstad, D., Bauerfeind, E., Nöthig, E. M., and Klages, M. (2010). Relationships between primary production and vertical particle export at the Atlantic-Arctic boundary (Fram Strait, HAUSGARTEN). *Polar Biol.* 33, 1733–1746. doi: 10.1007/s00300-010-0855-3

Fransson, A., Chierici, M., and Nojiri, Y. (2009). New insights into the spatial variability of the surface water carbon dioxide in varying sea ice conditions in the Arctic Ocean. *Cont. Shelf Res.* 29, 1317–1328. doi: 10.1016/j.csr.2009.03.008

Fransson, A., Chierici, M., Anderson, L. G., Bussmann, I., Kattner, G., Jones, E. P., et al. (2001). The importance of shelf processes for the modification of chemical constituents in the waters of the eastern Arctic Ocean. *Cont. Shelf Res.* 21, 225–242. doi: 10.1016/S0278-4343(00)00088-1

Fransson, A., Chierici, M., Skjelvan, I., Olsen, A., Assmy, P., Peterson, A. K., et al. (2017). Journal of Geophysical Research : Oceans high Arctic Ocean : Implications for sea-air CO 2 fluxes. *J. Geophysical Research: Oceans* 122 (7), 5566–5587. doi: 10.1002/2016JC012478

Ghaffari, P., Isachsen, P. E., Nøst, O. A., and Weber, J. E. (2018). The influence of topography on the stability of the Norwegian Atlantic Current off northern Norway. *J. Phys. Oceanography* 48 (11). doi: 10.1175/1520-0469

Graham, R. M., Itkin, P., Meyer, A., Sundfjord, A., Spreen, G., Smedsrud, L. H., et al. (2019). Winter storms accelerate the demise of sea ice in the Atlantic sector of the Arctic Ocean. *Sci. Rep.* 9, 9222. doi: 10.1038/s41598-019-45574-5

Haine, T. W., Curry, B., Gerdes, R., Hansen, E., Karcher, M., Lee, C., et al. (2015). Arctic freshwater export: Status, mechanisms, and prospects. *Global Planetary Change* 125, 13–35. doi: 10.1016/j.gloplacha.2014.11.013

Halvorsen, M. H., Smedsrud, L. H., Zhang, R., and Kloster, K. (2015). Fram Strait spring ice export and September Arctic sea ice. *Cryosphere Discussions* 9, 4205–4235. doi: 10.5194/tcd-9-4205-2015

Hattermann, T., Isachsen, P. E., von Appen, W. J., Albretsen, J., and Sundfjord, A. (2016). Eddy-driven recirculation of Atlantic water in Fram Strait. *Geophysical Res. Lett.* 43 (7). doi: 10.1002/2016GL068323

Håvik, L., Våge, K., Pickart, R. S., Harden, B., Appen, W. J. V., Jónsson, S., et al. (2017). Structure and variability of the shelfbreak East Greenland Current north of Denmark Strait. *J. Phys. Oceanography* 47 (10). doi: 10.1175/JPO-D-17-0062.1

Hofmann, Z., von Appen, W. J., and Wekerle, C. (2021). Seasonal and mesoscale variability of the two Atlantic water recirculation pathways in Fram Strait. *J. Geophysical Research: Oceans* 126 (7). doi: 10.1029/2020JC017057

Johnson, K. M., Wills, K. D., Butler, D. B., Johnson, W. K., and Wong, C. S. (2000). Coulometric total carbon dioxide analysis for marine studies: maximizing the performance of an automated gas extraction system and coulometric detector. *Mar. Chem.* 44, 1993, 167–187. doi: 10.1016/0304-4203(93)90201-X

Joli, N., Gosselin, M., Ardyna, M., Babin, M., Onda, D. F., Tremblay, J. É., et al. (2018). Need for focus on microbial species following ice melt and changing freshwater regimes in a Janus Arctic Gateway. *Sci. Rep.* 8, 1–11. doi: 10.1038/s41598-018-27705-6

Kahru, M., Brotas, V., Manzano-Sarabia, M., and Mitchell, B. G. (2011). Are phytoplankton blooms occurring earlier in the Arctic? *Global Change Biol.* 17, 1733–1739. doi: 10.1111/j.1365-2486.2010.02312.x

Karpouzoglou, T., de Steur, L., Smedsrud, L. H., and Sumata, H. (2022). Observed changes in the arctic freshwater outflow in fram strait. *J. Geophysical Research: Oceans* 127, 1–17. doi: 10.1029/2021JC018122

Kleypas, J. A. (2019). Impacts of ocean acidification on marine biodiversity. *Biodiversity Climate Change: Transforming Biosphere (Dic)*, 185–195. doi: 10.2307/j.ctv8jnzw1.25

Koziorowska-Makuch, K., Szymczycha, B., Thomas, H., and Kuliński, K. (2023). The marine carbonate system variability in high meltwater season (Spitsbergen Fjords, Svalbard). *Prog. Oceanography*, 211. doi: 10.1016/j.pocean.2023.102977

Krisch, S., Browning, T. J., Graeve, M., Ludwichowski, K. U., Lodeiro, P., Hopwood, M. J., et al. (2020). The influence of Arctic Fe and Atlantic fixed N on summertime primary production in Fram Strait, North Greenland Sea. *Sci. Rep.* 10, 1–13. doi: 10.1038/s41598-020-72100-9

Kuliński, K., Schneider, B., Szymczycha, B., and Stokowski, M. (2017). Structure and functioning of the acid-base system in the Baltic Sea. *Earth System Dynamics* 8, 1107–1120. doi: 10.5194/esd-8-1107-2017

Lalande, C., Bauerfeind, E., and Nöthig, E. M. (2011). Downward particulate organic carbon export at high temporal resolution in the eastern Fram Strait: influence of Atlantic Water on flux composition. *Mar. Ecol. Prog. Ser.*, 440. doi: 10.3354/meps09385

Lalande, C., Bauerfeind, E., Nöthig, E. M., and Beszczynska-Möller, A. (2013). Impact of a warm anomaly on export fluxes of biogenic matter in the eastern Fram Strait. *Prog. Oceanography* 109, 70–77. doi: 10.1016/j.pocean.2012.09.006

Lee, K., Kim, T. W., Byrne, R. H., Millero, F. J., Feely, R. A., and Liu, Y. M. (2010). The universal ratio of boron to chlorinity for the North Pacific and North Atlantic oceans. *Geochim. Cosmochim. Acta* 74, 1801–1811. doi: 10.1016/j.gca.2009.12.027

Lewis, K. M., Van Dijken, G. L., and Arrigo, K. R. (2020). Changes in phytoplankton concentration now drive increased Arctic Ocean primary production. *Science* 369, 198–202. doi: 10.1126/science.aay8380

Lewis, E., Wallace, D., and Allison, L. J. (1998). *Program developed for CO {sub 2} system calculations* (TN (United States: Brookhaven National Lab., Dept. of Applied Science, Upton, NY (United States); Oak Ridge National Lab., Carbon Dioxide Information Analysis Center). (No. ORNL/CDIAC-105).

Lueker, T. J., Dickson, A. G., and Keeling, C. D. (2000). Ocean pCO2 calculated from dissolved inorganic carbon, alkalinity, and equations for K1 and K2: validation based on laboratory measurements of CO2 in gas and seawater at equilibrium. *Mar. Chem.* 70 (1–3), 105–119.

MacGilchrist, G. A., Garabato, A. N., Tsubouchi, T., Bacon, S., Torres-Valdés, S., and Azetsu-Scott, K. (2014). The Arctic Ocean carbon sink. *Deep-Sea Res. Part I: Oceanographic Res. Papers* 86, 39–55. doi: 10.1016/j.dsr.2014.01.002

Manizza, M., Menemenlis, D., Zhang, H., and Miller, C. E. (2019). Modeling the recent changes in the arctic ocean CO2 sink, (2006–2013). *Global Biogeochemical Cycles* 33, 420–438. doi: 10.1029/2018GB006070

Marchese, C., de la Guardia, L. C., Myers, P. G., and Bélanger, S. (2019). Regional differences and inter-annual variability in the timing of surface phytoplankton blooms in the Labrador Sea. *Ecol. Indic.* 96, 81–90. doi: 10.1016/j.ecolind.2018.08.053

Marnela, M., Rudels, B., Houssais, M. N., Beszczynska-Möller, A., and Eriksson, P. B. (2013). Recirculation in the Fram Strait and transports of water in and north of the Fram Strait derived from CTD data. *Ocean Sci.* 9, 499–519. doi: 10.5194/os-9-499-2013

Mayot, N., Matrai, P. A., Arjona, A., Bélanger, S., Marchese, C., Jaegler, T., et al. (2020). Springtime export of arctic sea ice influences phytoplankton production in the Greenland sea. *J. Geophysical Research: Oceans* 125, 1–16. doi: 10.1029/2019JC015799

Mehrbach, C., Culberson, C. H., Hawley, J. E., and Pytkowicx, R. M. (1973). Measurement of the apparent dissociation constants of carbonic acid in seawater at atmospheric pressure 1. *Limnol. Oceanogr.* 18 (6). doi: 10.4319/lo.1973.18.6.0897

Meredith, M. P., Sommerkorn, M., Cassotta, S., Derksen, C., Ekaykin, A. A., Hollowed, A. B., et al. (2019). "Chapter 3: Polar Regions," in *The Ocean and Cryosphere in a Changing Climate: Summary for Policymakers*. Eds. O. Anisimov, G. Flato and C. Xiao (Monaco: Intergovernmental Panel on Climate Change), 3-1-3-173. Available online at: https://www.ipcc.ch/srocc/home/.

Middelburg, J. J., Soetaert, K., and Hagens, M. (2020). Ocean alkalinity, buffering and biogeochemical processes. *Rev. Geophysics* 58 (3), e2019RG000681. doi: 10.1029/2019RG000681

NASA Ocean Biology Processing Group (2023). *Moderate Resolution Imaging Spectroradiometer (Aqua-MODIS) Level-3 Monthly Chlorophyll concentration (4Km resolution).* Available online at: https://oceancolor.gsfc.nasa.gov/l3/ (Accessed 2023/02/29).

Nilsen, F., Skogseth, R., Vaardal-Lunde, J., and Inall, M. (2016). A simple shelf circulation model: intrusion of Atlantic Water on the West Spitsbergen Shelf. *J. Phys. Oceanography* 46 (4). doi: 10.1175/JPO-D-15-0058.1

Nilsen, F., Ersdal, E. A., and Skogseth, R. (2021). Wind-driven variability in the spitsbergen polar current and the svalbard branch across the yermak plateau. *J. Geophysical Research: Oceans* 126 (9), e2020JC016734. doi: 10.1029/2020JC016734

Nöthig, E. M., Bracher, A., Engel, A., Metfies, K., Niehoff, B., Peeken, I., et al. (2015). Summertime plankton ecology in fram strait-a compilation of long-and short-term observations. *Polar Res.* 34 (1), 23349. doi: 10.3402/polar.v34.23349

Orr, J. C., Epitalon, J. M., Dickson, A. G., and Gattuso, J. P. (2018). Routine uncertainty propagation for the marine carbon dioxide system. *Mar. Chem.* 207, 84–107. doi: 10.1016/j.marchem.2018.10.006

Pabi, S., van Dijken, G. L., and Arrigo, K. R. (2008). Primary production in the arctic ocean 1998-2006. *J. Geophysical Research: Oceans* 113, 1998–2006. doi: 10.1029/2007JC004578

Paulsen, M. L., Bratbak, G., Larsen, A., Seuthe, L., Egge, J. K., and Erga, S. R. (2017). *CarbonBridge 2014: Physical oceanography and microorganism composition during 5 cruises (Jan, March, May, August, Nov 2014) on and off the shelf northwest of Svalbard in 2014* (Center for Marine Environmental Sciences, University of Bremen (MARUM), Germany: PANGAEA). doi: 10.1594/PANGAEA.884255

Peng, G., Matthews, J. L., Wang, M., Vose, R., and Sun, L. (2020). What do global climate models tell us about future arctic sea ice coverage changes? *Climate* 8 (1), 15. doi: 10.3390/cli8010015

Perez, F. F., and Fraga, F. (1987). Association constant of fluoride and hydrogen ions in seawater. *Mar. Chem.* 21, 161–168. doi: 10.1016/0304-4203(87)90036-3

Polyakov, I. V., Timokhov, L. A., Alexeev, V. A., Bacon, S., Dmitrenko, I. A., Fortier, L., et al. (2010). Arctic Ocean warming contributes to reduced polar ice cap. *J. Phys. Oceanography* 40, 2743–2756. doi: 10.1175/2010JPO4339.1

Qi, D., Wu, Y., Chen, L., Cai, W. J., Ouyang, Z., Zhang, Y., et al. (2022). Rapid acidification of the arctic chukchi sea waters driven by anthropogenic forcing and biological carbon recycling. *Geophysical Res. Lett.* 49, 1–12. doi: 10.1029/2021GL097246

Raimondi, L., Matthews, J. B. R., Atamanchuk, D., Azetsu-Scott, K., and Wallace, D. W. (2019). The internal consistency of the marine carbon dioxide system for high latitude shipboard and *in situ* monitoring. *Mar. Chem.* 213, 49–70. doi: 10.1016/j.marchem.2019.03.001

Raj, R. P., Johannessen, J. A., Eldevik, T., Nilsen, J. Ø., and Halo, I. (2016). Quantifying mesoscale eddies in the Lofoten Basin. *J. Geophysical Research: Oceans* 121 (7). doi: 10.1080/01431161.2016.1201234

Richter, M. E., Von Appen, W. J., and Wekerle, C. (2018). Does the East Greenland Current exist in the northern Fram Strait? *Ocean Sci.* 14, 1147–1165. doi: 10.5194/os-14-1147-2018

Rippeth, T. P., Lincoln, B. J., Lenn, Y. D., Green, J. M., Sundfjord, A., and Bacon, S. (2015). Tide-mediated warming of Arctic halocline by Atlantic heat fluxes over rough topography. *Nat. Geosci.* 8, 191–194. doi: 10.1038/ngeo2350

Rudels, B., Björk, G., Nilsson, J., Winsor, P., Lake, I., and Nohr, C. (2005). The interaction between waters from the Arctic Ocean and the Nordic Seas north of Fram Strait and along the East Greenland Current: Results from the Arctic Ocean-02 Oden expedition. *J. Mar. Syst.* 55, 1–30. doi: 10.1016/j.jmarsys.2004.06.008

Rysgaard, S., Glud, R. N., Sejr, M. K., Bendtsen, J., and Christensen, P. B. (2007). Inorganic carbon transport during sea ice growth and decay: A carbon pump in polar seas. *J. Geophysical Research: Oceans* 112, 1–8. doi: 10.1029/2006JC003572

Saloranta, T. M., and Svendsen, H. (2001). Across the Arctic front west of Spitsbergen: high-resolution CTD sections from 1998–2000. *Polar Res.* 20, 177–184. doi: 10.3402/polar.v20i2.6515

Slagstad, D., Wassmann, P. F. J., and Ellingsen, I. (2015). Physical constrains and productivity in the future Arctic Ocean. *Front. Mar. Sci.* 2. doi: 10.3389/fmars.2015.00085

Schlitzer, R. (2023). *Ocean Data View, odv.awi.de.*

Spreen, G., Kaleschke, L., and Heygster, G. (2008). Sea ice remote sensing using AMSR-E 89-GHz channels. *J. Geophysical Research: Oceans* 113 (C2). doi: 10.1029/2005JC003384

Spreen, G., De Steur, L., and Divine, D. (2020). Arctic sea ice volume export through fram strait from 1992 to 2014. *J. Geophysical Research : Oceans*. 125 (6), e2019JC016039. doi: 10.1029/2019JC016039

Stokowski, M., Makuch, P., Rutkowski, K., Wichorowski, M., and Kuliński, K. (2021). A system for the determination of surface water pCO2 in a highly variable environment, exemplified in the southern Baltic Sea. *Oceanologia* 63 (2). doi: 10.1016/j.oceano.2021.01.001

Stroeve, J. C., Serreze, M. C., Holland, M. M., Kay, J. E., Malanik, J., and Barrett, A. P. (2012). The Arctic's rapidly shrinking sea ice cover: A research synthesis. *Climatic Change* 110, 1005–1027. doi: 10.1007/s10584-011-0101-1

Stroeve, J., and Notz, D. (2018). Changing state of Arctic sea ice across all seasons. *Environ. Res. Lett.* 13 (10), 103001. doi: 10.1088/1748-9326/aade56

Takahashi, T., Olafsson, J., Goddard, J. G., Chipman, D. W., and Sutherland, S. C. (1993). Seasonal variation of CO2 and nutrients in the high-latitude oceans: A comparative study. *Global Biogeochemical Cycles* 7, 843–878. doi: 10.1029/93GB02263

Takahashi, T., Sutherland, S. C., Sweeney, C., Poisson, A., Metzl, N., Tilbrook, B., et al. (2002). Global sea–air CO2 flux based on climatological surface ocean pCO2, and seasonal biological and temperature effects. *Deep Sea Res. Part II: Topical Stud. Oceanography* 49 (9-10). doi: 10.1016/S0967-0645(02)00003-6

Tremblay, J. É., Anderson, L. G., Matrai, P., Coupel, P., Bélanger, S., Michel, C., et al. (2015). Global and regional drivers of nutrient supply, primary production and CO2 drawdown in the changing Arctic Ocean. *Prog. Oceanography*. doi: 10.1016/j.pocean.2015.08.009

Trodahl, M., and Isachsen, P. E. (2018). Topographic influence on baroclinic instability and the mesoscale eddy field in the northern North Atlantic Ocean and the Nordic Seas. *J. Phys. Oceanography* 48 (11). doi: 10.1175/JPO-D-17-0220.1

Tsukernik, M., Deser, C., Alexander, M., and Tomas, R. (2010). Atmospheric forcing of Fram Strait sea ice export: A closer look. *Climate Dynamics* 35, 1349–1360. doi: 10.1007/s00382-009-0647-z

Tuerena, R. E., Hopkins, J., Buchanan, P. J., Ganeshram, R. S., Norman, L., von Appen, W. J., et al. (2021). An arctic strait of two halves: the changing dynamics of nutrient uptake and limitation across the fram strait. *Global Biogeochemical Cycles* 35, 1–20. doi: 10.1029/2021GB006961

Tynan, E., Clarke, J. S., Humphreys, M. P., Ribas-Ribas, M., Esposito, M., Rérolle, V. M., et al. (2016). Physical and biogeochemical controls on the variability in surface pH and calcium carbonate saturation states in the Atlantic sectors of the Arctic and Southern Oceans. *Deep-Sea Res. Part II: Topical Stud. Oceanography* 127, 7–27. doi: 10.1016/j.dsr2.2016.01.001

Vihma, T., Screen, J., Tjernström, M., Newton, B., Zhang, X., Popova, V., et al. (2016). The atmospheric role in the Arctic water cycle: A review on processes, past and future changes, and their impacts. *J. Geophysical Research: Biogeosciences* 121, 586–620. doi: 10.1002/2015JG003132

Wittmann, A. C., and Pörtner, H. O. (2013). Sensitivities of extant animal taxa to ocean acidification. *Nat. Climate Change* 3, 995–1001. doi: 10.1038/nclimate1982

Wolf-Gladrow, D. A., Zeebe, R. E., Klaas, C., Körtzinger, A., and Dickson, A. G. (2007). Total alkalinity: The explicit conservative expression and its application to biogeochemical processes. *Mar. Chem.* 106, 287–300. doi: 10.1016/j.marchem.2007.01.006

Woosley, R. J., and Millero, F. J. (2020). Freshening of the western Arctic negates anthropogenic carbon uptake potential. *Limnology Oceanography* 65, 1834–1846. doi: 10.1002/lno.11421

Woosley, R. J., Millero, F. J., and Takahashi, T. (2017). Internal consistency of the inorganic carbon system in the Arctic Ocean. *Limnology Oceanography: Methods* 15, 887–896. doi: 10.1002/lom3.10208

Yasunaka, S., Murata, A., Watanabe, E., Chierici, M., Fransson, A., van Heuven, S., et al. (2016). Mapping of the air–sea CO2 flux in the Arctic Ocean and its adjacent seas: Basin-wide distribution and seasonal to interannual variability. *Polar Sci.* 10, 323–334. doi: 10.1016/j.polar.2016.03.006

Yasunaka, S., Siswanto, E., Olsen, A., Hoppema, M., Watanabe, E., Fransson, A., et al. (2018). Arctic Ocean CO 2 uptake : an improved multiyear estimate of the air – sea CO 2 flux incorporating chlorophyll a concentrations. *Biogeosciences* 15 (6), 1643–1661. doi: 10.5194/bg-15-1643-2018

Yasunaka, S., Manizza, M., Terhaar, J., Olsen, A., Yamaguchi, R., Landschützer, P., et al. (2023). An assessment of CO2 uptake in the arctic ocean from 1985 to 2018. *Global Biogeochemical Cycles* 37, 1–27. doi: 10.1029/2023GB007806

Zhang, Y., Yamamoto-Kawai, M., and Williams, W. J. (2020). Two decades of ocean acidification in the surface waters of the beaufort gyre, arctic ocean: effects of sea ice melt and retreat from 1997–2016. *Geophysical Res. Lett.* 47, 1–11. doi: 10.1029/2019GL086421